Commun. Comput. Phys.
doi: 10.4208/cicp.OA-2025-0045

Vol. **39**, No. 1, pp. 261-295
January 2026

A Novel Structure-Preserving Algorithm with Green's Function Approach for Computing Band Structures of Photonic Quasicrystals

Tiexiang Li[1,3,*], Xing-Long Lyu[1], Ren-Cang Li[2] and Wen-Wei Lin[3]

[1] *School of Mathematics and Shing-Tung Yau Center, Southeast University, Nanjing 211189, People's Republic of China.*
[2] *Department of Mathematics, University of Texas at Arlington, Arlington, TX 76019-0408, USA.*
[3] *Shanghai Institute for Mathematics and Interdisciplinary Sciences, Shanghai 200433, People's Republic of China.*

Received 27 February 2025; Accepted (in revised version) 20 May 2025

Abstract. A novel bi-infinite approach to compute the band structures of 2D photonic superlattices with 1D quasicrystal sequences is devised. Leveraging strategically the bi-infinite characteristic, the approach first transforms the infinite-dimensional eigenvalue problem into a finite-dimensional nonlinear eigenvalue problem (NEVP) on a single cell for efficient numerical solution. Challengingly, the NEVP is built upon the solutions to two systems of cyclic nonlinear matrix equations (NMEs) that have to be solved repeatedly during iteratively solving the NEVP. The solutions are efficiently calculated by a newly developed highly efficient coalescing technique followed by a structure-preserving doubling algorithm. It is showed that the cost of coalescing is proportional to the logarithm of N, the length of the truncated quasicrystal sequence, which is significant as the cost of coalescing becomes more noticeable as N gets bigger for highly accurate simulations. Finally, through mathematical analysis, inclusion intervals for eigenvalue of interest are estimated so as to significantly narrow down the scope of search, and that significantly contributes to the overall efficiency of the approach, as the NEVP is nonlinear in nature and has to be solved iteratively.

AMS subject classifications: 65F15, 65M80, 65M60, 78M10

Key words: Photonic quasicrystal, photonic superlattice, nonlinear eigenvalue problem, cyclic structure-preserving algorithm, Fibonacci sequence.

*Corresponding author. *Email addresses:* txli@seu.edu.cn (T. Li), lxl_math@seu.edu.cn (X.-L. Lyu), rcli@uta.edu (R.-C. Li), wwlin@outlook.com (W.-W. Lin)

1 Introduction

Photonic quasicrystals (PQCs) [4, 23, 30], celebrated for their distinctive aperiodic order and intricate symmetries, have attracted considerable attention owing to their ability to manipulate light in novel ways. These structures present unique opportunities for directing photon flow, potentially advancing optical communication, sensing, and imaging technologies. Computational investigations of PQCs allow researchers to examine their bandgap properties and light propagation features, aiding the development of efficient photonic devices such as waveguides, lasers, and filters [22, 26, 34].

In the field of quasicrystal structure computation, the supercell approximation and projection methods are two of the most widely used techniques. These methods are crucial for simulating the complex aperiodic order inherent in photonic quasicrystals. The supercell approximation [24, 36, 39] constructs a sufficiently large periodic structure that mimics the quasicrystal, thereby enabling the use of traditional computational approaches. On the other hand, the projection method [13, 14, 25] maps low-dimensional photonic quasicrystals into a higher-dimensional periodic lattice, effectively capturing the aperiodic nature of quasicrystals. Both methods, however, require substantial computational resources to achieve high precision, as they must accurately account for complex interference patterns and subtle photonic bandgap effects. Consequently, enhancements in both computational power and algorithmic efficiency are vital for conducting detailed and accurate simulations, which are essential for designing optimally innovative photonic devices.

For approximating an 1D quasi-periodic structure using periodic structures, as shown in Fig. 1a, a supercell is a periodic unit created to contain as many cells as possible so that the quasi-periodic structure of interest is adequately approximated. There are two different ways to do so. One is to simply use a sufficiently large supercell and then repeats it, as in Fig. 1a where one supercell AB$\cdots$BA appears periodically. The other one which we will be using is to first select a central cell C (the *scattering region*) and then create two supercells, one for each sides of the scattering region, as shown in Fig. 1b where the scattering region is in the middle marked by C and to its left is supercell AB$\cdots$BA repeated and to its left is a different supercell AB$\cdots$AA repeated. This introduces an additional flexibility to account for different long-range periodic growths to the two sides of the scattering region, thereby reformulating the original model as an approximate bi-infinite one.

In this study, we focus on the band structure calculations for 2D photonic superlattice (PS) with 1D quasi-periodicity. By leveraging the supercell approximation, we employ a novel cyclic reduction technique to condense the computations involving large supercell structures into a manageable unit cell size. This means that even though a substantial number of supercells are necessary to approximate PS accurately, the actual dimension of the discrete eigenvalue problem remains relatively small when it comes to compute the band structure. This significantly reduces the computational complexity in the overall band structure calculation for 2D photonic superlattice, making it numerically efficient

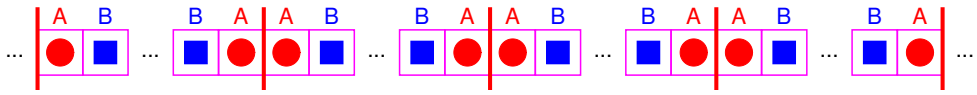

(a) Supercell AB···BA repeats periodically.

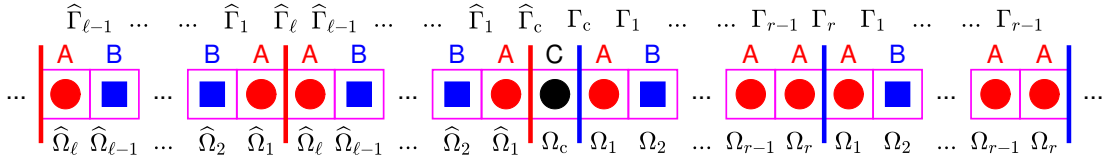

(b) Supercell AB···BA repeats periodically to the left of the central cell C (the scattering region), while, to its right, supercell AB···AA repeats periodically.

Figure 1: Periodic and bi-infinite approximants of photonic superlattice. In (b), cell C represents the scattering region, and $\Gamma_{\rm c}$, $\widehat{\Gamma}_{\rm c}$, $\{\Gamma_i\}_{i=1}^{r-1}$, $\{\widehat{\Gamma}_j\}_{j=1}^{\ell-1}$ represent interfaces between two related subdomains among $\Omega_{\rm c}$, $\{\Omega_i\}_{i=1}^{r}$, $\{\widehat{\Omega}_j\}_{j=1}^{\ell}$.

and practically feasible. The main contributions of this study are as follows.

- We approach the study of 2D photonic superlattices with 1D quasiperiodic properties from a novel bi-infinite perspective, which is akin but different from the classic periodic approximation. We utilize Green's function to transform the associated bi-infinite eigenvalue problem into a finite-dimensional nonlinear eigenvalue problem (NEVP), which is built upon the solutions to two systems of cyclic nonlinear matrix equations (NMEs) that have to be solved repeatedly during iteratively solving the NEVP.
- We adopt a cyclic scheme on the bi-infinite structure, leading to the development of a new cyclic structure-preserving doubling algorithm (C-SDA). C-SDA significantly accelerates the process of solving large-scale nonlinear matrix equations whose solutions are used to define the NEVP.
- Through mathematical analysis, we obtain inclusion intervals that contain the eigenvalues of interest, significantly narrowing down the scope of search and speeding up computations.

As a result, our method has a computational complexity of $\mathcal{O}(\log_\phi N)$ where N is the number of supercell utilized in the periodic approximant and ϕ is some irrational constant (i.e., $(\sqrt{5}+1)/2$ for Fibonacci) that characterizes the superlattice sequence, respectively. Compared to the commercial multiphysics software COMSOL[†], our method demonstrates significant advantages in speed and memory cost when the ultra-long periodic approximation of a quasi-periodic structure has to be used for highly accurate simulations.

[†]COMSOL Multiphisics® v 5.5.0, 2020, `https://www.comsol.com/`.

The rest of this paper is organized as follows. In Section 2, we introduce the mathematical model for 2D PS and our approach of using a bi-infinite perspective coupled with the finite element method (FEM) for discretization. In Section 3, we utilize the two-sided Schur complement approach to transform the discretized bi-infinite linear eigenvalue problem into a finite-dimensional NEVP. In Section 4, we explain our C-SDA to rapidly solve systems of cyclic NMEs. In Section 5 we first establish inclusive intervals for eigenvalues of interest and then explain a nonlinear variant of the Jacobi-Davidson method for to compute them. Section 6 estimates the overall complexity of our algorithm, and finally in Section 7 we report our numerical experiments to demonstrate the effectiveness and efficiency of our method. Conclusions are drawn in Section 8. There are two appendices. We provide a necessary review of The structure-preserving doubling algorithm is reviewed in Appendix A, along with some analysis particular to what we do in this paper. Appendix B derives determining equations for various derivatives that are needed by the Jacobi-Davidson method.

Notation. As usual, $\mathbb{R}$ and $\mathbb{C}$ are the sets of real and complex numbers, respectively, and $\mathbb{C}^{m\times n}$ is the set of all $m\times n$ complex matrices. X^{T} and X^* are the transpose and conjugate transpose of a matrix/vector X, respectively; $\sigma(X)$ and $\rho(X)$ denote the spectrum and spectral radius of a square matrix/linear operator X, respectively. The imaginary part of a square matrix X is defined as and denoted by $\mathrm{Im}(X) := (X-X^*)/(2\imath)$ where $\imath$ is the imaginary unit. $X \succ 0$ ($\succeq 0$) means that X is Hermitian, i.e., $X = X^*$ and positive definite (HPD) (Hermitian and positive semi-definite (HPSD)). For a column vector $\mathbf{v}$ (conventionally in bold lowercase), $\|\mathbf{v}\|_2 = \sqrt{\mathbf{v}^*\mathbf{v}}$.

2 Governing equations and finite element discretization

2.1 Governing equations

In the context of 2D electromagnetic models, electromagnetic waves can be classified into two principal types based on the orientation of the electric and magnetic fields: transverse magnetic (TM) modes and transverse electric (TE) modes. The TM modes are characterized by the electric field component being perpendicular to the plane of periodicity, commonly the xy-plane, with the magnetic field components residing within the plane. In contrast, the TE modes feature the magnetic field perpendicular to the plane of periodicity, while the electric field components are oriented within the plane. Each mode type delineates a distinct arrangement of electromagnetic fields as follows:

$$\begin{aligned} \textbf{TM modes:}\quad & E(\mathbf{r}) = (0,0,E_z(\mathbf{r})),\ H(\mathbf{r}) = (H_x(\mathbf{r}),H_y(\mathbf{r}),0),\\ \textbf{TE modes:}\quad & E(\mathbf{r}) = (E_x(\mathbf{r}),E_y(\mathbf{r}),0),\ H(\mathbf{r}) = (0,0,H_z(\mathbf{r})), \end{aligned}$$

where $\mathbf{r}$ is any point in the xy-plane.

In this paper, without loss of generality, we use the TE modes as the model of interest. By Maxwell's equations and the constitutive relations between electromagnetic fields in

PQCs, the band structure calculations of the TE modes of 2D PQCs can be, respectively, described by the Helmholtz eigenvalue problem (HEP)

$$-\nabla\cdot\left(\varepsilon_{\perp}^{-1}(\mathbf{r})\nabla H_z(\mathbf{r})\right)=\lambda\mu_z(\mathbf{r})H_z(\mathbf{r}),\quad \mathbf{r}\in\Omega, \tag{2.1}$$

where Ω is the domain of 2D PS, $\lambda\equiv\omega^2\in\mathbb{R}$ is the eigenvalue, $E_z(\mathbf{r})$ and $H_z(\mathbf{r})$ are the corresponding eigenfunctions,

$$\varepsilon(\mathbf{r})=\varepsilon_{\perp}(\mathbf{r})\oplus\varepsilon_z(\mathbf{r})\in\mathbb{C}^{2\times2}\oplus\mathbb{C},\quad \mu(\mathbf{r})=\mu_{\perp}(\mathbf{r})\oplus\mu_z(\mathbf{r})\in\mathbb{C}^{2\times2}\oplus\mathbb{C}$$

are the permittivity and the permeability, respectively, and both are block diagonal and HPD. Meanwhile, since the PQCs are assumed to be periodic along one of the two lattice translation vectors, the $\mathbf{a}_2$-direction, the electromagnetic fields along the $\mathbf{a}_2$-direction must satisfy the Bloch condition [17], i.e., H_z satisfies the quasi-periodic conditions along the $\mathbf{a}_2$ direction:

$$H_z(\mathbf{r}+\mathbf{a}_2)=e^{\imath 2\pi\mathbf{k}\cdot\mathbf{a}_2}H_z(\mathbf{r}),\quad \mathbf{r}\in\Omega, \tag{2.2}$$

where $2\pi\mathbf{k}$ is the Bloch wave vector within the first Brillouin zone [15].

2.2 Finite element discretization

Let $\mathbb{H}^1(\Omega)=\{f: f,\frac{\partial f}{\partial x},\frac{\partial f}{\partial y}\in L^2(\Omega)\}$. We define the Sobolev spaces

$$\begin{aligned}&C^{\infty}_{\mathrm{per}}(\Omega)=\{\phi\in C^{\infty}(\Omega):\phi(\mathbf{r}+\mathbf{a}_2)=\phi(\mathbf{r})\},\\&\mathbb{H}^1_{\mathrm{per}}(\Omega)=\text{the closure of } C^{\infty}_{\mathrm{per}}(\Omega)\text{ in }\mathbb{H}^1(\Omega).\end{aligned}$$

In addition, we define the quasi-periodic function space with respect to the lattice vector $\mathbf{a}_2$ for wave vector $\mathbf{k}\in\mathbb{R}^2$,

$$\mathbb{H}^{1,\mathbf{k}}_{\mathrm{per}}(\Omega)=\{\phi: e^{-\imath 2\pi\mathbf{k}\cdot\mathbf{a}_2}\phi\in\mathbb{H}^1_{\mathrm{per}}(\Omega),\ \mathbf{r}\in\Omega\}.$$

Therefore, for any $E_z,H_z,v\in C^{\infty}(\Omega)\cap\mathbb{H}^{1,\mathbf{k}}_{\mathrm{per}}(\Omega)$, with the periodic conditions (2.2), we have the weak formulation of HEP (2.1) [20] as

$$\int_{\Omega}\varepsilon_{\perp}^{-1}(\mathbf{r})\nabla H_z(\mathbf{r})\cdot\nabla v(\mathbf{r})d\Omega=\lambda\int_{\Omega}\mu_z(\mathbf{r})H_z(\mathbf{r})\cdot v(\mathbf{r})d\Omega. \tag{2.3}$$

We use the Galerkin-type finite element method (FEM) to approximate (2.3). Due to the structure of 2D PQCs as illustrated in Fig. 1b, we employ the same triangulation on the subdomains $\{\Omega_i\}_{i=1}^{r}$ and $\{\widehat{\Omega}_j\}_{j=1}^{\ell}$ in the same unit cells A or B. Let Γ_{i+1} be the interface between Ω_i and Ω_{i+1}, and $\widehat{\Gamma}_{j+1}$ the interface between $\widehat{\Omega}_j$ and $\widehat{\Omega}_{j+1}$.

Adopting the standard nodal bases $\{\phi_i\}_{i=1}^n$ of the finite element space $\mathbb{H}_{\rm per}^{1,\mathbf{k}}(\Omega_i)$ and $\mathbb{H}_{\rm per}^{1,\mathbf{k}}(\widehat{\Omega}_j)$, we obtain the FEM matrices in each subdomain as

$$K_i(s_i,t_i)=\int_{\Omega_i\backslash\Gamma_{i+1}}(\varepsilon_\perp^{-1}(\mathbf{r})\nabla\phi_{s_i}(\mathbf{r}))\cdot\nabla\phi_{t_i}(\mathbf{r})d\sigma, \tag{2.4a}$$

$$E_i(s_i,t_i)=\int_{\Gamma_{i+1}}(\varepsilon_\perp^{-1}(\mathbf{r})\nabla\phi_{s_i}(\mathbf{r}))\cdot\nabla\phi_{t_i}(\mathbf{r})d\sigma, \tag{2.4b}$$

$$M_i(s_i,t_i)=\int_{\Omega_i\backslash\Gamma_{i+1}}\mu_z(\mathbf{r})\phi_{s_i}(\mathbf{r})\cdot\phi_{t_i}(\mathbf{r})d\sigma, \tag{2.4c}$$

$$F_i(s_i,t_i)=\int_{\Gamma_{i+1}}\mu_z(\mathbf{r})\phi_{s_i}(\mathbf{r})\cdot\phi_{t_i}(\mathbf{r})d\sigma, \tag{2.4d}$$

$$\widehat{K}_j(\hat{s}_j,\hat{t}_j)=\int_{\widehat{\Omega}_j\backslash\widehat{\Gamma}_{j+1}}(\varepsilon_\perp^{-1}(\mathbf{r})\nabla\phi_{\hat{s}_j}(\mathbf{r}))\cdot\nabla\phi_{\hat{t}_j}(\mathbf{r})d\sigma, \tag{2.4e}$$

$$\widehat{E}_j(\hat{s}_j,\hat{t}_j)=\int_{\widehat{\Gamma}_{j+1}}(\varepsilon_\perp^{-1}(\mathbf{r})\nabla\phi_{\hat{s}_j}(\mathbf{r}))\cdot\nabla\phi_{\hat{t}_j}(\mathbf{r})d\sigma, \tag{2.4f}$$

$$\widehat{M}_j(\hat{s}_j,\hat{t}_j)=\int_{\widehat{\Omega}_j\backslash\widehat{\Gamma}_{j+1}}\mu_z(\mathbf{r})\phi_{\hat{s}_j}(\mathbf{r})\cdot\phi_{\hat{t}_j}(\mathbf{r})d\sigma, \tag{2.4g}$$

$$\widehat{F}_j(\hat{s}_j,\hat{t}_j)=\int_{\widehat{\Gamma}_{j+1}}\mu_z(\mathbf{r})\phi_{\hat{s}_j}(\mathbf{r})\cdot\phi_{\hat{t}_j}(\mathbf{r})d\sigma, \tag{2.4h}$$

where $i\in\{1,2,\cdots,r\}$, $j\in\{1,2,\cdots,\ell\}$, $s_i,t_i\in\{1,2,\cdots,n_i\}$ and $\hat{s}_j,\hat{t}_j\in\{1,2,\cdots,\hat{n}_j\}$ with n_i and $\hat{n}_j$ being the degrees of freedom (DoF) for each subdomains $\Omega_i\backslash\Gamma_{i+1}$ and $\widehat{\Omega}_j\backslash\widehat{\Gamma}_{j+1}$, respectively. It is understood that $K_i(s_i,t_i)$ in (2.4a) refers the (s_i,t_i)th entry of matrix K_i and the same understanding goes to the rest of expressions in (2.4).

For the central (scattering) region $\Omega_{\rm C}\backslash(\Gamma_{\rm C}\bigcup\widehat{\Gamma}_{\rm C})$, the corresponding discrete stiffness and mass matrices $K_{\rm C}$ and $M_{\rm C}$ are given by

$$K_{\rm C}(s_{\rm C},t_{\rm C})=\int_{\Omega_{\rm C}\backslash(\Gamma_{\rm C}\bigcup\widehat{\Gamma}_{\rm C})}(\varepsilon_\perp^{-1}(\mathbf{r})\nabla\phi_{s_{\rm C}}(\mathbf{r}))\cdot\nabla\phi_{t_{\rm C}}(\mathbf{r})d\sigma, \tag{2.5a}$$

$$M_{\rm C}(s_{\rm C},t_{\rm C})=\int_{\Omega_{\rm C}\backslash(\Gamma_{\rm C}\bigcup\widehat{\Gamma}_{\rm C})}\phi_{s_{\rm C}}(\mathbf{r})\cdot\phi_{t_{\rm C}}(\mathbf{r})d\sigma, \tag{2.5b}$$

respectively, where $s_{\rm C},t_{\rm C}\in\{1,2,\cdots,n_{\rm C}\}$, and $n_{\rm C}$ is the DoF for subdomain $\Omega_{\rm C}\backslash(\Gamma_{\rm C}\bigcup\widehat{\Gamma}_{\rm C})$. As in (2.4), the connection matrices $E_{\rm C}$ and $\widehat{E}_{\rm C}$ can be formulated by replacing the integration domain $\Omega_{\rm C}\backslash(\Gamma_{\rm C}\bigcup\widehat{\Gamma}_{\rm C})$ with $\Gamma_{\rm C}$ and $\widehat{\Gamma}_{\rm C}$ in (2.5a), respectively. The connection matrices $F_{\rm C}$ and $\widehat{F}_{\rm C}$ for the mass matrices are constructed in a similar way.

3 Eigenvalue problem for photonic quasicrystals

3.1 Green's function approach for the bi-infinite system

After HEP (2.1) for PQCs is discretized by the Galerkin-type FEM via the weak formulation (2.3), the corresponding submatrices in (2.4) and (2.5) are set up and integrated into

the so-called *Hamiltonian system* for PQCs, an infinite-dimensional matrix pencil $\mathcal{K}-\nu\mathcal{M}$, where both $\mathcal{K}$ and $\mathcal{M}$ are bi-infinite block tri-diagonal Hermitian matrices with $\mathcal{M}\succ 0$. Specifically, we have

$$\begin{aligned}\mathcal{K}&=\begin{bmatrix}\mathcal{K}_{\rm L} & \mathcal{E}_{\rm L,C} & \\ \mathcal{E}_{\rm L,C}^* & K_{\rm C} & \mathcal{E}_{\rm C,R}^* \\ & \mathcal{E}_{\rm C,R} & \mathcal{K}_{\rm R}\end{bmatrix},\\ \mathcal{M}&=\begin{bmatrix}\mathcal{M}_{\rm L} & \mathcal{F}_{\rm L,C} & \\ \mathcal{F}_{\rm L,C}^* & M_{\rm C} & \mathcal{F}_{\rm C,R}^* \\ & \mathcal{F}_{\rm C,R} & \mathcal{M}_{\rm R}\end{bmatrix},\end{aligned} \tag{3.1}$$

where $K_{\rm C}-\nu M_{\rm C}\in\mathbb{C}^{n_{\rm C}\times n_{\rm C}}$ is the Hamiltonian pencil for the central (scattering) region, $\mathcal{K}_{\rm R}-\nu\mathcal{M}_{\rm R}$ is the leading matrix pencil for PQCs corresponding to the right side to the scattering region C in Fig. 1b and has the following r-periodic leading block-tridiagonal structure:

$$\begin{aligned}\mathcal{K}_{\rm R}=&\begin{bmatrix}
K_1 & E_1^* & & & & & & \\
E_1 & \ddots & \ddots & & & & & \\
 & \ddots & K_{r-1} & E_{r-1}^* & & & & \\
 & & E_{r-1} & K_r & E_r^* & & & \\
 & & & E_r & K_1 & \ddots & & \\
 & & & & \ddots & \ddots & E_{r-1}^* & \\
 & & & & & E_{r-1} & K_r & \ddots \\
 & & & & & & \ddots & \ddots
\end{bmatrix}\\
=:&\,\mathrm{BTriD}\begin{bmatrix}K_1 & \cdots & K_{r-1} & K_r & K_1 & \cdots & K_r & \cdots\\ E_1 & \cdots & E_{r-1} & E_r & E_1 & \cdots & E_r & \cdots\end{bmatrix},\end{aligned} \tag{3.2a}$$

$$\mathcal{M}_{\rm R}=:\mathrm{BTriD}\begin{bmatrix}M_1 & \cdots & M_{r-1} & M_r & M_1 & \cdots & M_r & \cdots\\ F_1 & \cdots & F_{r-1} & F_r & F_1 & \cdots & F_r & \cdots\end{bmatrix}, \tag{3.2b}$$

$\mathcal{K}_{\rm L}-\nu\mathcal{M}_{\rm L}$ is the ending matrix pencil for PQCs corresponding to the left side to the scattering region C in Fig. 1b and has the following ℓ-periodic ending block-tridiagonal struc-

ture:

$$\mathcal{K}_{\mathrm{L}}=\begin{bmatrix}
\ddots & \ddots & & & & & & & \\
\ddots & \ddots & \widehat{E}_\ell^* & & & & & & \\
 & \widehat{E}_\ell & \widehat{K}_\ell & \ddots & & & & & \\
 & & \ddots & \ddots & \widehat{E}_1^* & & & & \\
 & & & \widehat{E}_1 & \widehat{K}_1 & \widehat{E}_\ell^* & & & \\
 & & & & \widehat{E}_\ell & \widehat{K}_\ell & \widehat{E}_{\ell-1}^* & & \\
 & & & & & \widehat{E}_{\ell-1} & \widehat{K}_{\ell-1} & \ddots & \\
 & & & & & & \ddots & \ddots & \widehat{E}_1^* \\
 & & & & & & & \widehat{E}_1 & \widehat{K}_1
\end{bmatrix}$$

$$=:\mathrm{BTriD}\begin{bmatrix}\cdots & \widehat{E}_\ell^* & \cdots & \widehat{E}_1^* & \widehat{E}_\ell^* & \widehat{E}_{\ell-1}^* & \cdots & \widehat{E}_1^*\\ \cdots & \widehat{K}_\ell & \cdots & \widehat{K}_1 & \widehat{K}_\ell & \widehat{K}_{\ell-1} & \cdots & \widehat{K}_1\end{bmatrix}, \tag{3.3a}$$

$$\mathcal{M}_{\mathrm{L}}=\mathrm{BTriD}\begin{bmatrix}\cdots & \widehat{F}_\ell^* & \cdots & \widehat{F}_1^* & \widehat{F}_\ell^* & \widehat{F}_{\ell-1}^* & \cdots & \widehat{F}_1^*\\ \cdots & \widehat{M}_\ell & \cdots & \widehat{M}_1 & \widehat{M}_\ell & \widehat{M}_{\ell-1} & \cdots & \widehat{M}_1\end{bmatrix}, \tag{3.3b}$$

and $\mathcal{E}_{\mathrm{L,C}}$, $\mathcal{E}_{\mathrm{C,R}}$, $\mathcal{F}_{\mathrm{L,C}}$ and $\mathcal{F}_{\mathrm{C,R}}$ are the associated conjuncting matrices:

$$\mathcal{E}_{\mathrm{C,R}}=\begin{bmatrix}E_{\mathrm{C}}^{\mathrm{T}},0,\cdots\end{bmatrix}^{\mathrm{T}},\qquad \mathcal{F}_{\mathrm{C,R}}=\begin{bmatrix}F_{\mathrm{C}}^{\mathrm{T}},0,\cdots\end{bmatrix}^{\mathrm{T}}, \tag{3.4a}$$

$$\mathcal{E}_{\mathrm{L,C}}=\begin{bmatrix}0,\cdots,0,\widehat{E}_{\mathrm{C}}^{\mathrm{T}}\end{bmatrix}^{\mathrm{T}},\quad F_{\mathrm{L,C}}=\begin{bmatrix}0,\cdots,0,\widehat{F}_{\mathrm{C}}^{\mathrm{T}}\end{bmatrix}^{\mathrm{T}}, \tag{3.4b}$$

with $E_{\mathrm{C}}-\nu F_{\mathrm{C}}$ and $\widehat{E}_{\mathrm{C}}-\nu\widehat{F}_{\mathrm{C}}$ coming from the boundary FEM discretization between the leading, the ending PQCs and the central region, respectively. Also in (3.2) and (3.3), $K_j-\nu M_j$ for $1\le j\le r$ and $\widehat{K}_j-\nu\widehat{M}_j$ for $1\le j\le\ell$ are squared matrix pencils with suitable sizes according to the interior FEM discretization as in (2.4), and $E_j-\nu F_j$ for $1\le j\le r$ and $\widehat{E}_j-\nu\widehat{F}_j$ for $1\le j\le\ell$ in (3.2) and (3.3) are rectangular matrix pencils of compatible sizes dictated by the boundary FEM discretization as in (2.4).

For later use, we define the following r-periodic leading block-tridiagonal matrices

$$\mathcal{K}_j=\mathrm{BTriD}\begin{bmatrix}K_j & \cdots & K_{r-1} & K_r & K_1 & \cdots & K_j & \cdots\\ E_j & \cdots & E_{r-1} & E_r & E_1 & \cdots & E_j & \cdots\end{bmatrix}, \tag{3.5a}$$

$$\mathcal{M}_j=\mathrm{BTriD}\begin{bmatrix}M_j & \cdots & M_{r-1} & M_r & M_1 & \cdots & M_j & \cdots\\ F_j & \cdots & F_{r-1} & F_r & F_1 & \cdots & F_j & \cdots\end{bmatrix}, \tag{3.5b}$$

for $1\le j\le r$, and the ℓ-periodic ending block-tridiagonal matrices

$$\widehat{\mathcal{K}}_j=\mathrm{BTriD}\begin{bmatrix}\cdots & \widehat{E}_j^* & \widehat{E}_{j-1}^* & \cdots & \widehat{E}_1^* & \widehat{E}_\ell^* & \cdots & \widehat{E}_j^*\\ \cdots & \widehat{K}_j & \widehat{K}_{j-1} & \cdots & \widehat{K}_1 & \widehat{K}_\ell & \cdots & \widehat{K}_j\end{bmatrix}, \tag{3.6a}$$

$$\widehat{\mathcal{M}}_j=\mathrm{BTriD}\begin{bmatrix}\cdots & \widehat{F}_j^* & \widehat{F}_{j-1}^* & \cdots & \widehat{F}_1^* & \widehat{F}_\ell^* & \cdots & \widehat{F}_j^*\\ \cdots & \widehat{M}_j & \widehat{M}_{j-1} & \cdots & \widehat{M}_1 & \widehat{M}_\ell & \cdots & \widehat{M}_j\end{bmatrix} \tag{3.6b}$$

for $1\leq j\leq \ell$. We now introduce Green's function approach [2,3,16] for the computation of band structures for PQCs. For any $\eta>0$, the infinite matrices $(\mathcal{K}_j-(\nu+\imath\eta)\mathcal{M}_j)$ and $\widehat{\mathcal{K}}_j-(\nu+\imath\eta)\widehat{\mathcal{M}}_j$ are known to be invertible because $\mathcal{K}_j-\nu\mathcal{M}_j$ and $\widehat{\mathcal{K}}_j-\nu\widehat{\mathcal{M}}_j$ can not have genuine complex eigenvalues. For $\nu^+:=\nu+\imath 0^+$, we let

$$(\mathcal{K}_j-\nu^+\mathcal{M}_j)^{-1}=\begin{bmatrix} G_j(\nu^+) & \cdots \\ \vdots & \ddots \end{bmatrix},\quad (\widehat{\mathcal{K}}_j-\nu^+\widehat{\mathcal{M}}_j)^{-1}=\begin{bmatrix} \ddots & \vdots \\ \cdots & \widehat{G}_j(\nu^+) \end{bmatrix}, \tag{3.7}$$

where $G_j(\nu^+)$ and $\widehat{G}_j(\nu^+)$ have the same sizes as K_j and $\widehat{K}_j$, respectively, and their existence and invertibility are guaranteed by [7, Chapter XXIV, Theorem 4.1] and [9]. Because of the periodic structures of the matrices in (3.5), recalling (3.7) and using the Schur complement technique, we find that, for $j=1,\cdots,r$,

$$G_j(\nu^+)=\Big[K_j-\nu M_j-(E_j-\nu F_j)^*G_{j+1}(\nu^+)(E_j-\nu F_j)\Big]^{-1}, \tag{3.8}$$

where $G_{r+1}(\cdot)=G_1(\cdot)$, a system of r cyclic nonlinear matrix equations (NMEs). Similarly, from (3.6) and (3.7) arises a system of ℓ cyclic NMEs: for $j=1,\cdots,\ell$,

$$\widehat{G}_j(\nu^+)=\Big[\widehat{K}_j-\nu\widehat{M}_j-(\widehat{E}_j-\nu\widehat{F}_j)\widehat{G}_{j+1}(\nu^+)(\widehat{E}_j-\nu\widehat{F}_j)^*\Big]^{-1}, \tag{3.9}$$

where $\widehat{G}_{\ell+1}(\cdot)=\widehat{G}_1(\cdot)$.

Performing Gauss elimination on $\mathcal{K}-\nu^+\mathcal{M}$ from the top and bottom with matrices $\mathcal{K}_{\rm L}-\nu^+\mathcal{M}_{\rm L}$ and $\mathcal{K}_{\rm R}-\nu^+\mathcal{M}_{\rm R}$ as pivoting matrices and recalling (3.1)-(3.3) and (3.7)-(3.9), we end up with the two-sided "Schur complement" of $K_{\rm C}-\nu M_{\rm C}$ at the central position as follows:

$$K_{\rm C}-\nu M_{\rm C}-(E_{\rm C}-\nu F_{\rm C})^*G_1(\nu^+)(E_{\rm C}-\nu F_{\rm C})-(\widehat{E}_{\rm C}-\nu\widehat{F}_{\rm C})\widehat{G}_1(\nu^+)(\widehat{E}_{\rm C}-\nu\widehat{F}_{\rm C})^*, \tag{3.10}$$

whose associated nonlinear eigenvalue problem (NEVP) is

$$\begin{aligned}\Big[K_{\rm C}-\nu M_{\rm C}-(E_{\rm C}-\nu F_{\rm C})^*G_1(\nu^+)(E_{\rm C}-\nu F_{\rm C}\\ -(\widehat{E}_{\rm C}-\nu\widehat{F}_{\rm C})\widehat{G}_1(\nu^+)(\widehat{E}_{\rm C}-\nu\widehat{F}_{\rm C})^*\Big]\mathbf{p}=0.\end{aligned} \tag{3.11}$$

A scalar-vector pair $(\nu,\mathbf{p})$ is called an eigenpair of the NEVP if it satisfies (3.11), and accordingly ν is called an eigenvalue and $\mathbf{p}$ the associated eigenvector. We point out that, by Green's function approach [3,17], only those eigenvalues ν such that $\{G_j(\nu^+)\}_{j=1}^r$ and $\{\widehat{G}_j(\nu^+)\}_{j=1}^\ell$ have nonzero imaginary parts are of interest.

3.2 Nonlinear eigenvalue problem for photonic superlattices

The bi-infinite generalized eigenvalue problem (GEP) for PQC structures by FEM can be formulated as

$$\mathcal{K}\mathbf{q}=\nu\mathcal{M}\mathbf{q}, \tag{3.12}$$

where $\mathcal{K}$ and $\mathcal{M}$ are as given in (3.1), $K_{\rm C}-\nu M_{\rm C}$ is the PQC for the central region, $M_{\rm C}\succeq 0$, $\mathcal{K}_{\rm R}-\nu\mathcal{M}_{\rm R}$ and $\mathcal{K}_{\rm L}-\nu\mathcal{M}_{\rm L}$ are the leading and ending matrix pencils for the PQC, approached by r and ℓ periodic leading and ending block-tridiagonal matrix pencils as given by (3.2) and (3.3), respectively. Let

$$L_{\rm C}(\nu^+)=(E_{\rm C}-\nu F_{\rm C})^* G_1(\nu^+)(E_{\rm C}-\nu F_{\rm C}), \tag{3.13a}$$
$$\widehat{L}_{\rm C}(\nu^+)=(\widehat{E}_{\rm C}-\nu\widehat{F}_{\rm C})\widehat{G}_1(\nu^+)(\widehat{E}_{\rm C}-\nu\widehat{F}_{\rm C})^*, \tag{3.13b}$$

where $G_1(\nu^+)$ and $\widehat{G}_1(\nu^+)$ are defined in (3.7). Then NEVP (3.11) can be written as

$$\left[K_{\rm C}-\nu M_{\rm C}-L_{\rm C}(\nu^+)-\widehat{L}_{\rm C}(\nu^+)\right]\mathbf{p}=0. \tag{3.14}$$

Let $\nu_{\rm C}$ be an isolated eigenvalue of $\mathcal{K}-\nu\mathcal{M}$ with eigenvector

$$\mathbf{q}\equiv\left[\mathbf{q}_{\rm L}^{\rm T},\mathbf{q}_{\rm C}^{\rm T},\mathbf{q}_{\rm R}^{\rm T}\right]^{\rm T}=\left[\cdots,\mathbf{q}_{-2}^{\rm T},\mathbf{q}_{-1}^{\rm T},\mathbf{q}_{\rm C}^{\rm T},\mathbf{q}_{1}^{\rm T},\mathbf{q}_{2}^{\rm T},\cdots\right]^{\rm T}.$$

We get, by (3.12),

$$\begin{bmatrix}\mathcal{K}_{\rm L} & \mathcal{E}_{\rm L,C} & \\ \mathcal{E}_{\rm L,C}^* & K_{\rm C} & \mathcal{E}_{\rm C,R}^* \\ & \mathcal{E}_{\rm C,R} & \mathcal{K}_{\rm R}\end{bmatrix}\begin{bmatrix}\mathbf{q}_{\rm L}\\ \mathbf{q}_{\rm C}\\ \mathbf{q}_{\rm R}\end{bmatrix}=\nu\begin{bmatrix}\mathcal{M}_{\rm L} & \mathcal{F}_{\rm L,C} & \\ \mathcal{F}_{\rm L,C}^* & M_{\rm C} & \mathcal{F}_{\rm C,R}^* \\ & \mathcal{F}_{\rm C,R} & \mathcal{M}_{\rm R}\end{bmatrix}\begin{bmatrix}\mathbf{q}_{\rm L}\\ \mathbf{q}_{\rm C}\\ \mathbf{q}_{\rm R}\end{bmatrix}. \tag{3.15}$$

In the following theorem, we will establish a connection between the bi-infinite GEP (3.12) and NEVP (3.11) or equivalently NEVP (3.14).

Theorem 3.1. *If* $(\nu_{\rm C},[\mathbf{q}_{\rm L}^{\rm T},\mathbf{q}_{\rm C}^{\rm T},\mathbf{q}_{\rm R}^{\rm T}]^{\rm T})$ *is an eigenpair of* $\mathcal{K}-\nu\mathcal{M}$*, i.e., satisfying* (3.15)*, then* $(\nu_{\rm C},\mathbf{q}_{\rm C})$ *is an eigenpair of NEVP* (3.14)*, i.e.,*

$$\left[K_{\rm C}-\nu_{\rm C}M_{\rm C}-L_{\rm C}(\nu_{\rm C})-\widehat{L}_{\rm C}(\nu_{\rm C})\right]\mathbf{q}_{\rm C}=0. \tag{3.16}$$

Proof. Expand (3.15) to get

$$\mathcal{K}_{\rm L}\mathbf{q}_{\rm L}+\mathcal{E}_{\rm L,C}\mathbf{q}_{\rm C}=\nu_{\rm C}(\mathcal{M}_{\rm L}\mathbf{q}_{\rm L}+\mathcal{F}_{\rm L,C}\mathbf{q}_{\rm C}), \tag{3.17a}$$
$$\mathcal{E}_{\rm C,R}\mathbf{q}_{\rm C}+\mathcal{K}_{\rm R}\mathbf{q}_{\rm R}=\nu_{\rm C}(\mathcal{F}_{\rm C,R}\mathbf{q}_{\rm C}+\mathcal{M}_{\rm R}\mathbf{q}_{\rm R}), \tag{3.17b}$$
$$\mathcal{E}_{\rm L,C}^*\mathbf{q}_{\rm L}+K_{\rm C}\mathbf{q}_{\rm C}+\mathcal{E}_{\rm C,R}^*\mathbf{q}_{\rm R}=\nu_{\rm C}(\mathcal{F}_{\rm L,C}^*\mathbf{q}_{\rm L}+M_{\rm C}\mathbf{q}_{\rm C}+\mathcal{F}_{\rm C,R}^*\mathbf{q}_{\rm R}). \tag{3.17c}$$

Solve (3.17a) and (3.17b) for $\mathbf{q}_{\rm L}$ and $\mathbf{q}_{\rm R}$ to get

$$\mathbf{q}_{\rm L}=-(\mathcal{K}_{\rm L}-\nu_{\rm C}\mathcal{M}_{\rm L})^{-1}(\mathcal{E}_{\rm L,C}-\nu_{\rm C}\mathcal{F}_{\rm L,C})\mathbf{q}_{\rm C}, \tag{3.18a}$$
$$\mathbf{q}_{\rm R}=-(\mathcal{K}_{\rm R}-\nu_{\rm C}\mathcal{M}_{\rm R})^{-1}(\mathcal{E}_{\rm C,R}-\nu_{\rm C}\mathcal{F}_{\rm C,R})\mathbf{q}_{\rm C}. \tag{3.18b}$$

Plugging $\mathbf{q}_{\mathrm{L}}$ and $\mathbf{q}_{\mathrm{R}}$ in (3.18) into (3.17c) yields

$$\begin{aligned}0=&(K_{\mathrm{C}}-\nu_{\mathrm{C}}M_{\mathrm{C}})\mathbf{q}_{\mathrm{C}}+(\mathcal{E}_{\mathrm{L,C}}-\nu_{\mathrm{C}}\mathcal{F}_{\mathrm{L,C}})^*\mathbf{q}_{\mathrm{L}}+(\mathcal{E}_{\mathrm{C,R}}-\nu_{\mathrm{C}}\mathcal{F}_{\mathrm{C,R}})^*\mathbf{q}_{\mathrm{R}}\\ =&[K_{\mathrm{C}}-\nu_{\mathrm{C}}M_{\mathrm{C}}-(\mathcal{E}_{\mathrm{L,C}}-\nu_{\mathrm{C}}\mathcal{F}_{\mathrm{L,C}})^*(\mathcal{K}_{\mathrm{L}}-\nu_{\mathrm{C}}\mathcal{M}_{\mathrm{L}})^{-1}(\mathcal{E}_{\mathrm{L,C}}-\nu_{\mathrm{C}}\mathcal{F}_{\mathrm{L,C}})\\ &-(\mathcal{E}_{\mathrm{C,R}}-\nu_{\mathrm{C}}\mathcal{F}_{\mathrm{C,R}})^*(\mathcal{K}_{\mathrm{R}}-\nu_{\mathrm{C}}\mathcal{M}_{\mathrm{R}})^{-1}(\mathcal{E}_{\mathrm{C,R}}-\nu_{\mathrm{C}}\mathcal{F}_{\mathrm{C,R}})]\mathbf{q}_{\mathrm{C}}.\end{aligned}\tag{3.19}$$

By (3.4) and (3.7), (3.19) becomes

$$\Big[K_{\mathrm{C}}-\nu_{\mathrm{C}}M_{\mathrm{C}}-(\widehat{E}_{\mathrm{C}}-\nu_{\mathrm{C}}\widehat{F}_{\mathrm{C}})\widehat{G}_1(\nu_{\mathrm{C}})(\widehat{E}_{\mathrm{C}}-\nu_{\mathrm{C}}\widehat{F}_{\mathrm{C}})^*-(E_{\mathrm{C}}-\nu_{\mathrm{C}}F_{\mathrm{C}})^*G_1(\nu_{\mathrm{C}})(E_{\mathrm{C}}-\nu_{\mathrm{C}}F_{\mathrm{C}})\Big]\mathbf{q}_{\mathrm{C}}=0,$$

which is the same as (3.16), upon noticing (3.13). □

As a consequence of Theorem 3.1, for the study the band structures for PQCs on the central region, it suffices to consider NEVP:

$$\begin{aligned}F_{\mathrm{C}}(\nu)\mathbf{q}_{\mathrm{C}}:=\Big[&K_{\mathrm{C}}-\nu M_{\mathrm{C}}-(\widehat{E}_{\mathrm{C}}-\nu\widehat{F}_{\mathrm{C}})\widehat{G}_1(\nu)(\widehat{E}_{\mathrm{C}}-\nu_{\mathrm{C}}\widehat{F}_{\mathrm{C}})^*\\ &-(E_{\mathrm{C}}-\nu F_{\mathrm{C}})^*G_1(\nu)(E_{\mathrm{C}}-\nu F_{\mathrm{C}})\Big]\mathbf{q}_{\mathrm{C}}=0,\end{aligned}\tag{3.20}$$

which unfortunately is built upon $G_1(\nu)$ and $\widehat{G}_1(\nu)$, the solutions to the systems of cyclic NMEs (3.8) and (3.9), respectively, and they are not explicitly available.

4 Cyclic SDA for a system of cyclic NMEs

In subsection 3.2, we have reduced the bi-infinite GEP (3.12) to a finite dimensional NEVP (3.20). This NEVP is defined in terms of $G_1(\nu)$ and $\widehat{G}_1(\nu)$, solutions to the two systems of cyclic NMEs (3.8) and (3.9), respectively. Both $G_1(\nu)$ and $\widehat{G}_1(\nu)$ depend on ν, and when NEVP (3.20) is solved iteratively, such as by the nonlinear Jacobi-Davidson method [35] that we will be using, they have to be computed repeatedly for many different ν. Therefore it is imperative to be able to solve these cyclic NMEs efficiently and accurately. To that end, we propose a fast method that consists of two stages:

1. Given ν, each of the two systems of cyclic NMEs is coalesced into one NME of the form
$$X=Q-A^*(X-P)^{-1}A,\tag{4.1}$$
where $A,P,Q\in\mathbb{C}^{n\times n}$, $P=P^*$ and $Q=Q^*$;
2. Solve NME (4.1) by the structure-preserving doubling algorithm (SDA) [10–12].

For ease of reference, we will call this two-staged method *Cyclic SDA* (C-SDA).

In the rest of this section, we focus on the first stage: coalescing, and leave a detailed account of SDA for (4.1) to Appendix A.

To coalesce either (3.8) or (3.9) into one NME, we first reformulate them in terms of $\big[G_j(\nu^+)\big]^{-1}$ and $\big[\widehat{G}_j(\nu^+)\big]^{-1}$, respectively, as follows: for $j=1,\cdots,r$,

$$G_j(\nu^+)^{-1}=K_j-\nu M_j-(E_j-\nu F_j)^*\big[G_{j+1}(\nu^+)^{-1}\big]^{-1}(E_j-\nu F_j), \tag{4.2}$$

where $G_{r+1}(\cdot)=G_1(\cdot)$, and, for $j=1,\cdots,\ell$,

$$\widehat{G}_j(\nu^+)^{-1}=\widehat{K}_j-\nu\widehat{M}_j-(\widehat{E}_j-\nu\widehat{F}_j)\big[\widehat{G}_{j+1}(\nu^+)^{-1}\big]^{-1}(\widehat{E}_j-\nu\widehat{F}_j)^*, \tag{4.3}$$

where $\widehat{G}_{\ell+1}(\cdot)=\widehat{G}_1(\cdot)$.

The basic idea of coalescing either (3.8) or (3.9) can be best explained by merging the following two NMEs

$$X_a=Q_a-A_a^*(X_b-P_a)^{-1}A_a, \tag{4.4a}$$
$$X_b=Q_b-A_b^*(X_c-P_b)^{-1}A_b, \tag{4.4b}$$

into one through eliminating X_b, where X_a, X_b, and X_c are unknown square matrices but otherwise may have different sizes among them, and the sizes of all other matrices in (4.4) are conformably determined by the involved matrix operations, e.g., P_a has the same size as X_b. Substitute (4.4b) into (4.4a), with the help of the Sherman-Morrison-Woodbury formula, to get

$$\begin{aligned}
X_a&=Q_a-A_a^*\big[Q_b-A_b^*(X_c-P_b)^{-1}A_b-P_a\big]^{-1}A_a\\
&=Q_a-A_a^*\big[(Q_b-P_a)^{-1}\\
&\quad+(Q_b-P_a)^{-1}A_b^*\big(X_c-P_b-A_b(Q_b-P_a)^{-1}A_b^*\big)^{-1}A_b(Q_b-P_a)^{-1}\big]A_a\\
&=\big[Q_a-A_a^*(Q_b-P_a)^{-1}A_a\big]\\
&\quad-\big[A_a^*(Q_b-P_a)^{-1}A_b^*\big]\big[X_c-\big(P_b+A_b(Q_b-P_a)^{-1}A_b^*\big)\big]^{-1}A_b(Q_b-P_a)^{-1}A_a,
\end{aligned} \tag{4.5}$$

or a new NME

$$X_a=Q_{(ab)}-A_{(ab)}^*(X_c-P_{(ab)})^{-1}A_{(ab)}, \tag{4.6}$$

without X_b, where

$$Q_{(ab)}=Q_a-A_a^*(Q_b-P_a)^{-1}A_a, \tag{4.7a}$$
$$P_{(ab)}=P_b+A_b(Q_b-P_a)^{-1}A_b^*, \tag{4.7b}$$
$$A_{(ab)}=A_b(Q_b-P_a)^{-1}A_a. \tag{4.7c}$$

Suppose that now we are given r-cyclic NMEs as

$$X_j=Q_j-A_j^*(X_{j+1}-P_j)^{-1}A_j,\quad j=1,\cdots,r, \tag{4.8}$$

where $X_{r+1}=X_1$ and each X_j is a square matrix and two different X_j may have different sizes, and the sizes of all other involved matrices are determined accordingly by the

involved matrix operations. A general way to coalesce (4.8) goes as follows. First we eliminate X_2, X_4, $\cdots$, i.e., all X_j with even indices by merging the jth equation into the $(j-1)$st equation. If r is odd, the last equation remains untouched. In the end, we get $\lceil r/2\rceil$-cyclic NMEs in $X_1, X_3, \cdots, X_{\lceil r/2\rceil}$. Repeat the process until only one NME, in the form (4.1) in X_1 only, remains, at which point SDA becomes applicable to compute X_1, and if necessary, $X_r, X_{r-1}, \cdots, X_2$ can be obtained by evaluating the right-hand side of the equations in (4.8) backwards.

In applying the reduction process above to (4.2), for given $\nu^+ := \nu + \imath 0^+$, we turn it into (4.8), with identifications:

$$X_j = \left[G_j(\nu^+)\right]^{-1}, \quad A_j = E_j - \nu F_j, \quad Q_j = K_j - \nu M_j, \quad P_j = 0, \tag{4.9}$$

for $j = 1, \cdots, r$. For the case of (4.3), we turn it into (4.8), with identifications:

$$X_j = \left[\widehat{G}_j(\nu^+)\right]^{-1}, \quad A_j^* = \widehat{E}_j - \nu \widehat{F}_j, \quad Q_j = \widehat{K}_j - \nu \widehat{M}_j, \quad P_j = 0, \tag{4.10}$$

for $j = 1, \cdots, \ell$, and $r = \ell$.

What we have just explained is for a general system (4.8) of cyclic NMEs, without paying any attention to if some of the coalescing operations are identical and thus do not have to be done more than once. For our purpose in this paper, i.e., coalescing (4.2) and (4.3), there are indeed quite a lot of identical coalescing operations. We shall now explain. Commonly used in one-dimensional quasiperiodic sequences are the Fibonacci sequence, Octonacci sequence, and Thue-Morse sequence, *etc*. which are composed of two different types of cells arranged in a specific order as a result of their peculiar substitution rules:

- Fibonacci sequence: substitution rule is

$$\begin{bmatrix} A \\ B \end{bmatrix} \quad \to \quad \begin{bmatrix} 1 & 1 \\ 1 & 0 \end{bmatrix} \begin{bmatrix} A \\ B \end{bmatrix} = \begin{bmatrix} AB \\ A \end{bmatrix}.$$

  As an example, we get $A \to AB \to ABA \to ABAAB \to ABAABABA \to ABAABABAABAAB \to \cdots$

- Octonacci sequence: substitution rule is

$$\begin{bmatrix} A \\ B \end{bmatrix} \quad \to \quad \begin{bmatrix} 2 & 1 \\ 1 & 0 \end{bmatrix} \begin{bmatrix} A \\ B \end{bmatrix} = \begin{bmatrix} AAB \\ A \end{bmatrix}.$$

  As an example, we get $B \to A \to AAB \to AABAABA \to AABAABAAABAABAAAB \to \cdots$

- Thue-Morse sequence: substitution rule is

$$\begin{bmatrix} A \\ B \end{bmatrix} \quad \to \quad \begin{bmatrix} 1 & 1 \\ 1 & 1 \end{bmatrix} \begin{bmatrix} A \\ B \end{bmatrix} = \begin{bmatrix} AB \\ AB \end{bmatrix}.$$

  As an example, we get $A \to AB \to ABBA \to ABBABAAB \to ABBABAABBAABABBA \to \cdots$

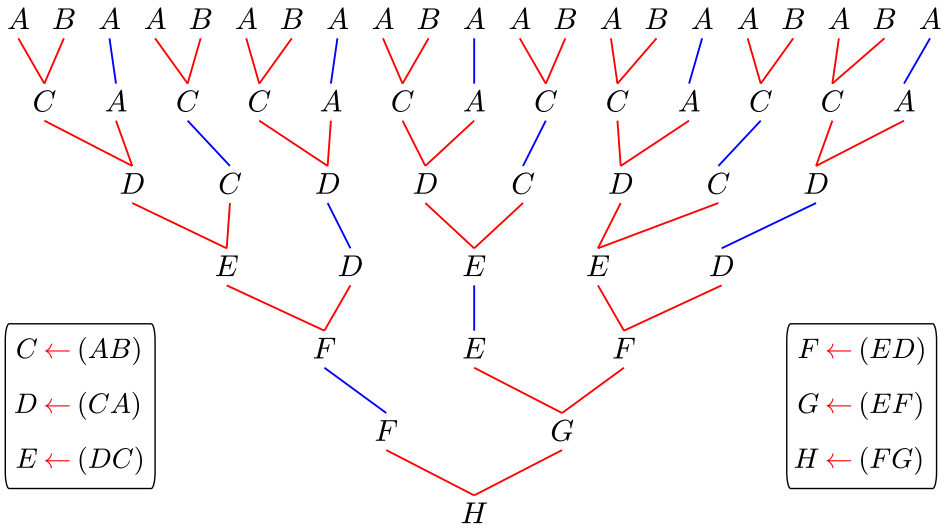

Figure 2: Coalescing scheme for a truncated Fibonacci sequence.

Coalescing cyclic NMEs (4.8) is done by sweeps until there is only one NME in the form of (4.1). During each sweep, there are many pairwise repetitions, as shown in Fig. 2 for coalescing a truncated Fibonacci sequence. In the figure, we see 8 coalescing transformation $AB \to C$ in the first sweep, 5 coalescing transformation $CA \to D$ in the second sweep, 3 coalescing transformation $DC \to E$ in the third sweep, 2 coalescing transformation $ED \to F$ in the fourth sweep, and finally just one coalescing transformation $EF \to G$ and $FG \to H$ in the fifth and sixth sweeps, respectively. Computationally, all coalescing transformations of the same type are exactly the same and do not need to be repeated and, as a result, there is only one coalescing transformation to do per sweep! That amounts to a huge saving. It is important to note that the 6 coalescing sweeps are intimately linked to the property of the Fibonacci sequence. Indeed, the number of coalescing sweeps 6, is derived from $\log_{\phi_F} 21 \approx 6$, where $\phi_F \approx 1.618$ is the golden ratio. In general for a truncated Fibonacci sequence, the number of coalescing sweeps required to reduce it to a sequence of length 1 is approximately $\log_{\phi_F} N$. Similarly, for truncated Octonacci and Thue-Morse sequences of length N, the numbers of coalescing sweeps required are approximately $\log_{\phi_O} N$ and $\log_{\phi_T} N$, respectively, where $\phi_O \approx 2.414$ for Octonacci and $\phi_T = 2$ for Thue-Morse.

5 Solve NEVP (3.20)

We are now ready to solve NEVP (3.20). We will use a nonlinear variation [35] of the Jacobi-Davidson method (JD) [27,28] to calculate eigenvalues of interest. Previously we mentioned that solving NEVP (3.20) iteratively requires repeatedly evaluating $G_1(\cdot)$ and

$\widehat{G}_1(\cdot)$. This will be accomplished by C-SDA, which first coalesces the systems (4.2) and (4.3) of NMEs, respectively, to yield two independent NMEs

$$[G_1(\theta)]^{-1} = Q_\alpha(\theta) - A_\alpha(\theta)^*\big([G_1(\theta)]^{-1} - P_\alpha(\theta)\big)^{-1}A_\alpha(\theta), \tag{5.1a}$$

$$[\widehat{G}_1(\theta)]^{-1} = \widehat{Q}_\alpha(\theta) - \widehat{A}_\alpha(\theta)\big([\widehat{G}_1(\theta)]^{-1} - \widehat{P}_\alpha(\theta)\big)^{-1}\widehat{A}_\alpha(\theta)^*, \tag{5.1b}$$

in $G_1(\cdot)$ and $\widehat{G}_1(\cdot)$, respectively, and then solve them independently via SDA which is reviewed in Appendix A.

In general, to find all eigenvalues of interest such as the first many smallest eigenvalues, we will have to search extensively and blindly within a large interval. That can be costly and ineffective. To overcome that, we will first establish inclusion intervals that contain eigenvalues of interest in Subsection 5.1 before we discuss the JD method for solving NEVP (3.20) in Subsection 5.2.

5.1 Inclusion intervals for ν^+ of interest

Previously we commented, after (3.11), that we need to determine those ν^+ so that $\mathrm{Im}(G_1(\nu^+)) \neq 0$ or $\mathrm{Im}(\widehat{G}_1(\nu^+)) \neq 0$. Recall the matrices K_i, E_i, M_i, F_i, and $\widehat{K}_j$, $\widehat{E}_j$, $\widehat{M}_j$, $\widehat{F}_j$ from FEM in Subsection 2.2. Let

$$\begin{aligned} C &= C_d - \lambda^{-1}C_c - \lambda C_c^* \\ &\equiv \begin{bmatrix} K_1 & & 0 \\ & \ddots & \\ 0 & & K_r \end{bmatrix} - \lambda^{-1}\begin{bmatrix} E_1 & & & E_r \\ & \ddots & & \\ & & E_{r-1} & \end{bmatrix} - \lambda\begin{bmatrix} & E_1^* & & \\ & & \ddots & \\ & & & E_{r-1}^* \\ E_r^* & & & \end{bmatrix}, \end{aligned} \tag{5.2a}$$

$$\begin{aligned} D &= D_d - \lambda^{-1}D_c - \lambda D_c^* \\ &\equiv \begin{bmatrix} M_1 & & 0 \\ & \ddots & \\ 0 & & M_r \end{bmatrix} - \lambda^{-1}\begin{bmatrix} F_1 & & & F_r \\ & \ddots & & \\ & & F_{r-1} & \end{bmatrix} - \lambda\begin{bmatrix} & F_1^* & & \\ & & \ddots & \\ & & & F_{r-1}^* \\ F_r^* & & & \end{bmatrix}, \end{aligned} \tag{5.2b}$$

$$\begin{aligned} \widehat{C} &= \widehat{C}_d - \lambda^{-1}\widehat{C}_c - \lambda\widehat{C}_c^* \\ &\equiv \begin{bmatrix} \widehat{K}_\ell & & 0 \\ & \ddots & \\ 0 & & \widehat{K}_1 \end{bmatrix} - \lambda^{-1}\begin{bmatrix} & \widehat{E}_{\ell-1} & & \\ & & \ddots & \\ \widehat{E}_\ell & & & \widehat{E}_1 \end{bmatrix} - \lambda\begin{bmatrix} & & & \widehat{E}_\ell \\ \widehat{E}_{\ell-1} & & & \\ & \ddots & & \\ & & \widehat{E}_1 & \end{bmatrix}, \end{aligned} \tag{5.2c}$$

$$\begin{aligned}\widehat{D}&=\widehat{D}_d-\lambda^{-1}\widehat{D}_c-\lambda\widehat{D}_c^*\\&\equiv\begin{bmatrix}\widehat{M}_\ell & & 0\\ & \ddots & \\ 0 & & \widehat{M}_1\end{bmatrix}-\lambda^{-1}\begin{bmatrix} & & \widehat{F}_{\ell-1}\\ & \iddots & \\ \widehat{F}_\ell & & \end{bmatrix}-\lambda\begin{bmatrix}\widehat{F}_\ell & & \\ & \ddots & \\ & & \widehat{F}_1\end{bmatrix}.\end{aligned}\tag{5.2d}$$

Since $\mathcal{M}\succ 0$ in (3.1), we know $D,\widehat{D}\succ 0$ by [1, Theorem 3.1] and [5, Theorem 2.1] and hence the eigenvalues of matrix pencils $C-\nu D$ and $\widehat{C}-\nu\widehat{D}$ are real. Let

$$A=C_c-\nu D_c,\quad Q=C_d-\nu D_d,\quad \widehat{A}=\widehat{C}_c-\nu\widehat{D}_c,\quad \widehat{Q}=\widehat{C}_d-\nu\widehat{D}_d,\tag{5.3}$$

and consider NMEs

$$X=Q-A^*X^{-1}A,\quad \widehat{X}=\widehat{Q}-\widehat{A}^*\widehat{X}^{-1}\widehat{A}.\tag{5.4}$$

The first NME in (5.4) and the system (4.2) of cyclic NMEs are closely related, and the same can be said about the second NME there and the system (4.3) of cyclic NMEs.

Denote the unit circle in the complex plane by $\mathbb{T}$. For $\lambda\in\mathbb{T}$ and $\nu\in\mathbb{R}$, denote the eigenvalues of matrix pencils $C-\nu D$ and $\widehat{C}-\nu\widehat{D}$ as defined in (5.2) by

$$\nu_1(\lambda)\le\cdots\le\nu_m(\lambda),\quad \widehat{\nu}_1(\lambda)\le\cdots\le\widehat{\nu}_{\widehat{m}}(\lambda),$$

respectively. Let, for $i=1,\cdots,m$, and $j=1,\cdots,\widehat{m}$,

$$\Delta_i=\Big[\min_{|\lambda|=1}\nu_i(\lambda),\max_{|\lambda|=1}\nu_i(\lambda)\Big],\quad \widehat{\Delta}_j=\Big[\min_{|\lambda|=1}\widehat{\nu}_j(\lambda),\max_{|\lambda|=1}\widehat{\nu}_j(\lambda)\Big],\tag{5.5a}$$

$$\Delta=(\bigcup_{i=1}^{m}\Delta_i)\bigcup(\bigcup_{i=1}^{\widehat{m}}\widehat{\Delta}_i).\tag{5.5b}$$

With these preparation, we are ready to state our inclusion theorem for eigenvalues of interest.

Theorem 5.1. *Suppose the unimodular eigenvalues (if any) of the quadratic eigenvalue problems (QEPs) for $Q-\lambda^{-1}A-\lambda A^*$ and $\widehat{Q}-\lambda^{-1}\widehat{A}-\lambda\widehat{A}^*$ are semi-simple. Then $\nu\in\Delta$ if and only if the QEPs for $(Q_\alpha-P_\alpha)-\lambda^{-1}A_\alpha-\lambda A_\alpha^*$ and $(\widehat{Q}_\alpha-\widehat{P}_\alpha)-\lambda^{-1}\widehat{A}_\alpha-\lambda\widehat{A}_\alpha^*$ associated with the leading and ending NMEs in* (5.1) *have some eigenvalues on $\mathbb{T}$, which is equivalent to that* $\mathrm{Im}(G_1(\nu^+))\neq 0$ *and* $\mathrm{Im}(\widehat{G}_1(\nu^+))\neq 0$.

Proof. For $\nu\in\Delta$, it holds that

$$\begin{aligned}0&=\det(C-\nu D)=\det\big((C_d-\lambda^{-1}C_c-\lambda C_c^*)-\nu(D_d-\lambda^{-1}D_c-\lambda D_c^*)\big)\\&=\det\big((C_d-\nu D_d)-\lambda^{-1}(C_c-\nu D_c)-\lambda(C_c^*-\nu D_c^*)\big)\\&=\det(Q-\lambda^{-1}A-\lambda A^*),\end{aligned}$$

where A and Q are as defined in (5.3). Since the QEP for $Q-\lambda^{-1}A-\lambda A^*$ has some semi-simple eigenvalues $\lambda\in\mathbb{T}$, NME $X=Q-A^*X^{-1}A$ has a unique weakly stable solution X with $\mathrm{Im}(X)\neq 0$ [11]. Furthermore, the associated NME $X=Q-A^*X^{-1}A$, related to the system (4.2) of cyclic NMEs (see also (4.8) with (4.9)), is equivalent to the symplectic GEP

$$\begin{bmatrix} A & 0 \\ Q & -I \end{bmatrix}\begin{bmatrix} I \\ X \end{bmatrix}=\begin{bmatrix} 0 & I \\ A^* & 0 \end{bmatrix}\begin{bmatrix} I \\ X \end{bmatrix}S,$$

where $X=\mathrm{diag}(G_1(\nu^+)^{-1},\cdots,G_r(\nu^+)^{-1})$ with $\mathrm{Im}(X)\neq 0$,

$$S=\begin{bmatrix} & & & S_r \\ S_1 & & & \\ & \ddots & & \\ & & S_{r-1} & \end{bmatrix}$$

with $S_j=X_{j+1}^{-1}A_j$, $j=1,\cdots,r$ and $X_1=X_{r+1}$, and $\sigma(S)\subset\{\lambda\in\mathbb{C}:|\lambda|\leq 1\}$. Thus the associated QEP for $(Q_\alpha-P_\alpha)-\lambda^{-1}A_\alpha-\lambda A_\alpha^*$ with (5.1a) at the completion of coalescing also has some eigenvalues $\lambda\in\mathbb{T}$, and so the weakly stable solution $G_1(\nu^+)^{-1}$ to (5.1a) must have nonzero imaginary part, which is equivalent to $\mathrm{Im}(G_1(\nu^+))\neq 0$. That $\mathrm{Im}(\widehat{G}_1(\nu^+))\neq 0$ can be proved analogously. □

Remark 5.1. In Theorem 5.1, it has been shown that $\mathrm{Im}(G_1(\nu^+))\neq 0$ and $\mathrm{Im}(\widehat{G}_1(\nu^+))\neq 0$ for $\nu\in\Delta$. Thus, the eigenvalue band structure of interest of NEVP (3.20) lies inside the union of intervals $\{\Delta_i\}_{i=1}^m$ and $\{\widehat{\Delta}_i\}_{i=1}^{\widehat{m}}$ in (5.5).

5.2 Jacobi-Davidson method for the NEVP

In this subsection, we apply the nonlinear variation [35] of the Jacobi-Davidson method to solve NEVP (3.20), in which the corresponding matrix-valued functions $G_1(\cdot)$ and $\widehat{G}_1(\cdot)$ will be evaluated by C-SDA as explained in Section 4.

Let $(\theta,\mathbf{v})$ be an approximate eigenpair of (3.20), the JD correction is determined by [35]

$$\begin{cases} \left[I-F_{\mathrm{C}}'(\theta)\mathbf{v}\mathbf{u}^*\right]F_{\mathrm{C}}(\theta)(I-\mathbf{v}\mathbf{v}^*)\mathbf{t}=-F_{\mathrm{C}}(\theta)\mathbf{v}=:-\mathbf{r}, \\ \mathbf{t}\perp\mathbf{v}, \\ \mathbf{u}^*F_{\mathrm{C}}'(\theta)\mathbf{v}=1. \end{cases} \tag{5.6}$$

Let $\epsilon=\mathbf{u}^*F_{\mathrm{C}}(\theta)\mathbf{t}$ to be determined. Then from (5.6) it follows that

$$\mathbf{t}=\epsilon F_{\mathrm{C}}(\theta)^{-1}F_{\mathrm{C}}'(\theta)\mathbf{v}-F_{\mathrm{C}}(\theta)^{-1}\mathbf{r}. \tag{5.7}$$

Use $\mathbf{v}^*\mathbf{t}=0$ to get

$$\epsilon=\mathbf{v}^*F_{\mathrm{C}}(\theta)^{-1}\mathbf{r}/\left(\mathbf{v}^*F_{\mathrm{C}}(\theta)^{-1}F_{\mathrm{C}}'(\theta)\mathbf{v}\right). \tag{5.8}$$

Once ϵ is calculated by (5.8), the correction vector $\mathbf{t}$ can be computed according to (5.7), but for that we will need to calculate $F_{\mathrm{C}}'(\theta)$ and solve two linear systems

$$F_{\mathrm{C}}(\theta)\mathbf{y}=\mathbf{r},\quad F_{\mathrm{C}}(\theta)\mathbf{z}=F_{\mathrm{C}}'(\theta)\mathbf{v} \tag{5.9}$$

for $\mathbf{y}=F_{\mathrm{C}}(\theta)^{-1}\mathbf{r}$ and $\mathbf{z}=F_{\mathrm{C}}(\theta)^{-1}\big[F_{\mathrm{C}}'(\theta)\mathbf{v}\big]$.

In Appendix B, we have derived a formula for $F_{\mathrm{C}}'(\theta)$ which involves not only $G_1(\theta)$ and $\widehat{G}_1(\theta)$ but also their derivatives $G_1'(\theta)$ and $\widehat{G}_1'(\theta)$. Previously in Section 4, we explained how to evaluate $G_1(\theta)$ and $\widehat{G}_1(\theta)$ via C-SDA. It turns out that evaluating $G_1'(\theta)$ and $\widehat{G}_1'(\theta)$ requires solving two systems of cyclic Stein equations which in turn can be also be done similarly to the methodology of C-SDA: 1) coalesce the two systems of cyclic Stein equations into two independent Stein equations, respectively, 2) solve the two Stein equations by Smith's method [29, 37]. As described, computing $F_{\mathrm{C}}'(\theta)$ this way is not cheap. Ultimately, we opt to approximate $F_{\mathrm{C}}'(\theta)$ by forward divided-difference:

$$F_{\mathrm{C}}'(\theta)\approx\frac{F_{\mathrm{C}}(\theta+\delta\theta)-F_{\mathrm{C}}(\theta)}{\delta\theta}$$

throughout our numerical experiments and it works well and is efficient.

According to (3.20), we have

$$\begin{aligned}F_{\mathrm{C}}(\theta)=K_{\mathrm{C}}-\theta M_{\mathrm{C}}&-(\widehat{E}_{\mathrm{C}}-\theta\widehat{F}_{\mathrm{C}})^{*}\widehat{G}_1(\theta)(\widehat{E}_{\mathrm{C}}-\theta\widehat{F}_{\mathrm{C}})\\&-(E_{\mathrm{C}}-\theta F_{\mathrm{C}})^{*}G_1(\theta)(E_{\mathrm{C}}-\theta F_{\mathrm{C}}),\end{aligned} \tag{5.10}$$

where $G_1(\theta)$ and $\widehat{G}_1(\theta)$ can be calculated by SDA on (5.1). Note that since the size of NEVP (3.20) is modest, the two linear systems in (5.9) can simply be solved by one Gaussian elimination on $F_{\mathrm{C}}(\theta)$.

One step of the JD method is locally equivalent to one Newton step and, for that reason, the JD iteration is usually quadratically convergent. Furthermore, after one eigenvalue is converged, we use the locking and purging strategy in [27, 35] to compute other eigenvalues.

Finally, we integrate all algorithmic ingredients explained so far together to yield our complete algorithm for the band structure computation in Algorithm 1, which we will name as FAME$_{\mathrm{PQC}}$, an extension of our previous fast algorithms for photonic crystals [21, 33], specifically designed for computing the band structures of PQCs with 1D quasi-periodicity.

6 Computational complexity

Let $N=\max\{r,\ell\}$, where r and ℓ are the lengths of the cyclic NMEs (3.8) and (3.9). In view of previous discussions, we need to perform approximately $\log_\phi N$ coalescing operations to merge the cyclic NMEs into independent ones in the form of (4.1), where ϕ is the generating ratio of the sequence of interest, e.g., $\phi=1.618$ for Fibonacci, 2.414 for Octonacci,

Algorithm 1 FAME$_{\text{PQC}}$: A Green's function based structure-preserving algorithm with Jacobi-Davidson iteration for calculating band structures of photonic quasicrystals

Input: lattice translation vectors $\mathbf{a}_1$, $\mathbf{a}_2$, permittivity ε, permeability μ, information of the 1D quasi-periodicity for 2D PQCs.

Output: eigenvalues $\{\omega_i\}_{i=1}^m$ of NEVP (3.20).

1: construct K_i, M_i, E_i, F_i $i=1,\cdots,r$, and $\widehat{K}_j, \widehat{M}_j, \widehat{E}_j, \widehat{F}_j$ for $j=1,\cdots,\ell$ according to (2.4) and $K_{\text{C}}, M_{\text{C}}, E_{\text{C}}, F_{\text{C}}$ according to (2.5);

2: pick initial guesses to potential eigenvalues in the intervals estimated according to Theorem 5.1, and then employ the nonlinear Jacobi-Davidson method to solve NEVP (3.20) with the correction formula as in (5.6), keeping in mind that, during the Jacobi-Davidson iteration, the evaluations of $G_1(\cdot)$ and $\widehat{G}_1(\cdot)$ are done by applying Algorithm A.2 (C-SDA) to solve (4.2) and (4.3), respectively.

and 2 for Thue-Morse. The resulting NME (4.1) is then solved by a few SDA iterations. Since matrices originating from FEM within each cell are relatively sparse, and matrices $E_i - \nu F_i$ arising from discretizing the interfaces between different cells are of very high sparsity, the computational complexity of each coalescing step is approximately $\mathcal{O}(n^2)$, where n is merely the discretization scale of the scattering cell (i.e., the size of K_{C}). Therefore, the overall computational complexity of coalescing cyclic NMEs (4.2) and (4.3) is approximately $(\log_\phi N)\mathcal{O}(n^2)$, the dominant cost of the whole computing procedure.

For maintaining high approximation accuracy, it is often necessary to go for a sufficiently fine grid within each single cell, which in turn leads to a large discretization scale n for the single cell. At this point, further subdivision of a cell can be performed, say through breaking it up into p parts, which accordingly reduces the size of the matrices involved in the SDA iterations. It is important to note that such an action will increase the length of the sequence, for example, turning an original sequence of $ABAAB$ into $A_1\cdots A_pB_1\cdots B_pA_1\cdots A_pA_1\cdots A_pB_1\cdots B_p$. However, the overall computational complexity is actually reduced. In fact, the subdivision roughly reduces the matrix size from n to n/p while the number of merging operations increases from $\log_\phi N$ to $2(p-1)+\log_\phi N$ due to $2(p-1)$ more steps for merging $A_1\cdots A_p$ and $B_1\cdots B_p$ into A and B separately first before the inherent characteristics of the original sequence can be taken advantage of as showcased in Fig. 2. Since each merging costs $\mathcal{O}((n/p)^2)$, the total computational cost is now about $\frac{2(p-1)+\log_\phi N}{p^2}\mathcal{O}(n^2)$.

7 Numerical experiments

In this section, we demonstrate the correctness and efficiency of our proposed method FAME$_{\text{PQC}}$ as outlined in Algorithm 1 for calculating 2D PQCs through several numerical experiments, and compare it with COMSOL, the commercial multiphysics software for simulating real-world designs, devices, and processes. We use Fibonacci, Octonacci,

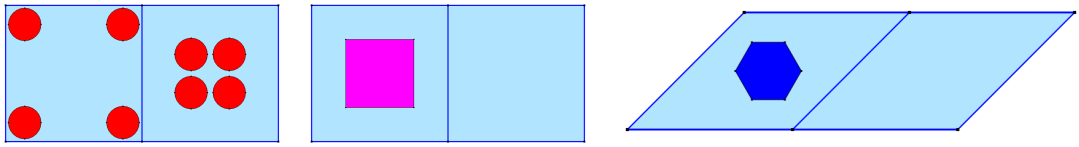

(a) A and B for Fibonacci. (b) A and B for Octonacci. (c) A and B for Thue-Morse.

Figure 3: Geometric schematics of cells A and B for Fibonacci, Octonacci and Thue-Morse sequences.

and Thue-Morse sequences as examples, whose specific generating rules are detailed in Section 4. The model parameters for our experiments are as follows (the lattice constant $a=20$ mm for all):

- Fibonacci sequence (Su-Schrieffer-Heeger model in [32,38]). Lattice translation vectors are $\mathbf{a}_1=a[1,0]^{\mathrm{T}}$, $\mathbf{a}_2=a[0,1]^{\mathrm{T}}$. Cells A and B each contains four circular dielectrics of radius $0.12a$ in the square shape with the side lengths $0.72a$ and $0.28a$, respectively, as shown in Fig. 3a. Each dielectric has relative permittivity $\varepsilon_r=6.1$ and relative permeability $\mu_r=1$.
- Octonacci sequence. Lattice translation vectors are $\mathbf{a}_1=a[1,0]^{\mathrm{T}}$, $\mathbf{a}_2=a[0,1]^{\mathrm{T}}$. Cell A contains 1 square dielectric with side length $0.5a$ while cell B is blank, as shown in Fig. 3b. The square dielectric has relative permittivity $\varepsilon_r=6.1$ and relative permeability $\mu_r=1$.
- Thue-Morse sequence. Lattice translation vectors are $\mathbf{a}_1=a[1,0]^{\mathrm{T}}$, $\mathbf{a}_2=a[\frac{\sqrt{2}}{2},\frac{\sqrt{2}}{2}]^{\mathrm{T}}$. Cell A contains 1 normal hexagonal dielectric with side length $0.2a$ while cell B is blank, as shown in Fig. 3c. The hexagonal dielectric has relative permittivity $\varepsilon_r=4$ and relative permeability $\mu_r=1$.

We implement the nonlinear Jacobi-Davidson method in Section 5 in MATLAB[‡] to compute a small number of positive eigenvalues. The tolerances for Jacobi-Davidson and SDA are set to 10^{-10} and 10^{-12}, respectively. All calculations are performed in MATLAB R2023b or by COMSOL Multiphysics on a workstation with 64 GB of memory and an Intel(R) Core(TM) i7-10700K @ 3.80 GHz processor in IEEE double precision arithmetic.

The weak form (2.3) of HEP (2.1) is discretized by FEM. In the first two experiments, We begin by truncating the Fibonacci/Octonacci/Thue-Morse sequence to one with length N and then extend this truncated sequence periodically to the left and right of the central region, as in Fig. 1b, and hence, $r=\ell=N$. In the third experiment, we aim to demonstrate the versatility of our approach in handling different long-range periodic growths to the two sides of the scattering region whereas COMSOL cannot.

[‡]The MathWorks®, `https://www.mathworks.com/products/matlab.html`.

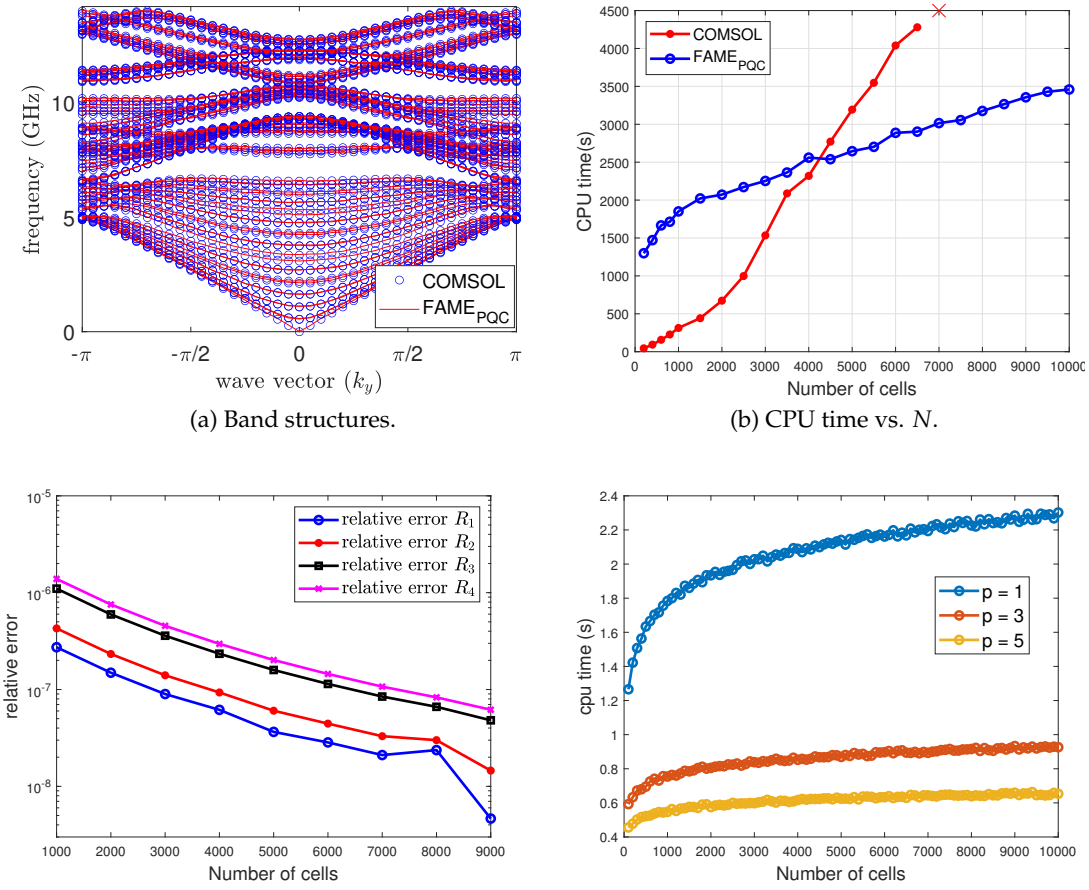

(a) Band structures.

(b) CPU time vs. N.

(c) Relative errors vs. N.

(d) CPU time for C-SDA.

Figure 4: Numerical results by COMSOL and by FAME$_{\text{PQC}}$ for the truncated Fibonacci sequence: (a) Band structures (calculated with $N=20$); (b) CPU time vs. N with $\mathbf{k}=[0,0]$ and $p=1$; (c) Relative error R_j as defined in (7.1) vs. N; (d) Time vs. N with $\mathbf{k}=[0,0]$ and $p=1,3,5$.

The FEM matrices, $K_{\text{C}}-\nu M_{\text{C}}$, $E_{\text{C}}-\nu F_{\text{C}}$, and $\widehat{E}_{\text{C}}-\nu\widehat{F}_{\text{C}}$, as detailed in (3.1), along with $K_j-\nu M_j$, $E_j-\nu F_j$ for $j=1,\cdots,r$ in (3.2), and $\widehat{K}_j-\nu\widehat{M}_j$, $\widehat{E}_j-\nu\widehat{F}j$ for $j=1,\cdots,\ell$ in (3.3), are computed for subdomains Ω_{C}, $\{\Omega_i\}_{i=1}^{r}$, $\{\widehat{\Omega}_j\}_{j=1}^{\ell}$ and boundaries Γ_{C}, $\widehat{\Gamma}_{\text{C}}$, $\{\Gamma_i\}_{i=1}^{r-1}$, $\{\widehat{\Gamma}_j\}_{j=1}^{\ell-1}$ according to (2.4). Lastly, we solve NEVP (3.20) associated with the band structure for PQCs within the central region C in Fig. 1b by FAME$_{\text{PQC}}$.

Experiment 1: Consider the 2D PS with 1D Fibonacci sequence. We seek the 100 smallest eigenvalues of NEVP (3.20): $F_{\text{C}}(\nu)\mathbf{q}_{\text{C}}=0$. Our numerical results are shown in Fig. 4 which has four subplots:

Fig. 4a: The band structures of the 30 smallest eigenvalues ω of (3.20) are plotted against the second component of the Bloch vector $\mathbf{k}$, with $r=\ell=N=20$. The band structures computed by both COMSOL and FAME$_{\text{PQC}}$ show excellent agreement.

Fig. 4b: CPU time by FAME$_{\text{PQC}}$ and COMSOL are plotted as the length of the truncated sequence length N varies. It shows that COMSOL has an advantage for N less than 4000 but runs slower than Algorithm 1 for N bigger than 4000. It is important to notice that COMSOL quickly becomes infeasible. The observation can be well explained. For relative small N, the discrete matrix is relative small in size and at the same time the potential of the coalescing strategy in FAME$_{\text{PQC}}$ has not been fully realized yet. When N is very large, exceeding 4000 for the case, FAME$_{\text{PQC}}$ demonstrates a clear speed advantage due to the fact that the logarithmic compression effect become increasingly significant. Moreover, for the case when N exceeds 7000, due to high memory requirement, COMSOL can no longer complete its calculations, whereas our FAME$_{\text{PQC}}$ can still go forward up to $N=10000$.

Fig. 4c: The relative errors in the first five computed eigenvalues ω are plotted. These eigenvalues clearly depends on N. For that reason, we shall write the jth eigenvalue as $\omega_j(N)$. It can be justified that $N\cdot\omega_j(N)$ approaches a constant as N increases. For that reason, we define the relative error R_j for the jth eigenvalue $\omega_j(\cdot)$ in Fig. 4c as

$$\text{relative error}\quad R_j(N_i):=\frac{|N_{i+1}\omega_j(N_{i+1})-N_i\omega_j(N_i)|}{N_i\omega_j(N_i)}, \tag{7.1}$$

where $N_i=i\cdot 10^3$.

Fig. 4d: We subdivide each unit cell, A and B, into p parts, i.e., A_1, A_2, $\cdots$, A_p and B_1, B_2, $\cdots$, B_p, to observe the computational performance of FAME$_{\text{PQC}}$ as p varies. To illustrate the effect of p, we plot CPU time by C-SDA for a single Jacobi-Davidson iteration in Fig. 4d. It can be observed that CPU time is logarithmically related to N, consistent with the analysis in Section 6.

Experiment 2: Similarly, consider 2D PQCs with 1D Octonacci and Thue-Morse sequences, respectively. We also compute their band structures by FAME$_{\text{PQC}}$ and by COMSOL. The results are displayed in Fig. 5a and Fig. 6a, showing that the band structures by the two methods are in full agreement.

Fig. 5b and Fig. 6b show CPU time by FAME$_{\text{PQC}}$ and by COMSOL for Octonacci and Thue-Morse, respectively. We observe a similar trend: COMSOL holds an edge for small N and loses out big as N increases for the same reason as we explained in the first experiment. Additionally, for $N>8000$, COMSOL aborts due to out of memory on the workstation.

Experiment 3: We combine the truncated Fibonacci sequence with the same physical parameters as in Fig. 3a and with ℓ=13 and a truncated Octonacci sequence with the same

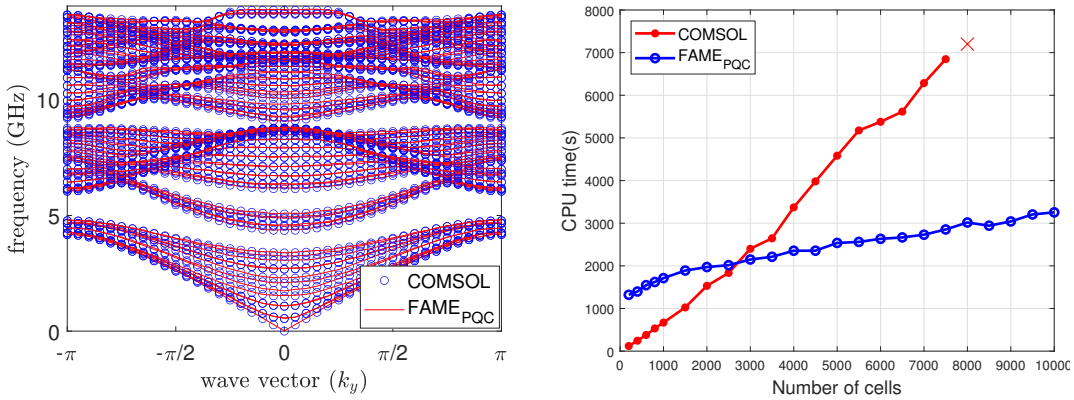

(a) Band structures. (b) CPU time vs. N.

Figure 5: Numerical results by COMSOL and by FAME$_{PQC}$ for the truncated Octonacci sequence: (a) Band structures (calculated with $N=20$); (b) CPU time vs. N with $\mathbf{k}=[0,0]$ and $p=1$.

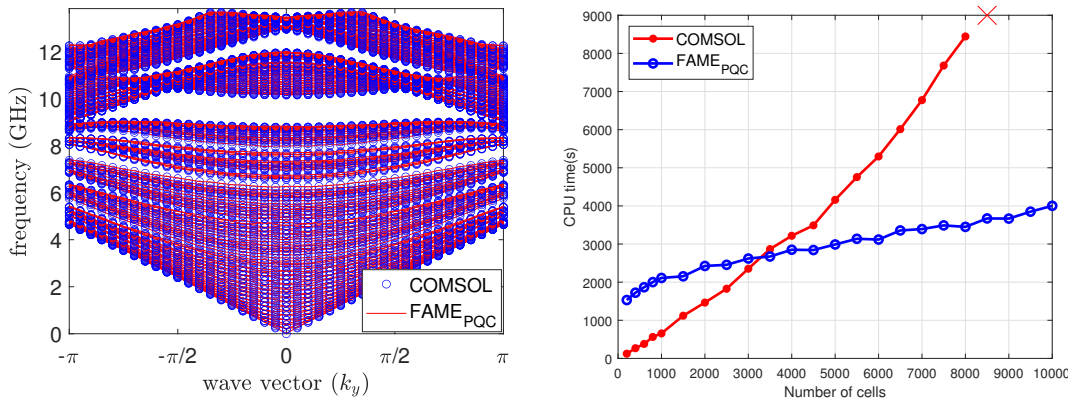

(a) Band structures. (b) CPU time vs. ρ_F.

Figure 6: Numerical results by COMSOL and by FAME$_{PQC}$ for the truncated Thue-Morse sequence: (a) Band structures (calculated with $N=20$); (b) CPU time vs. N with $\mathbf{k}=[0,0]$ and $p=1$.

physical parameters as in Fig. 3b and with $r=17$, as the left and right parts, respectively, to create a bi-infinite approximants of photonic superlattice as in Fig. 1b. COMSOL cannot deal with such a configuration while our FAME$_{PQC}$ can. After computing the smallest 200 positive eigenvalues, we obtained the band structure of such a photonic quasicrystal, as shown in Fig. 7 plots the band structure computed by FAME$_{PQC}$ for the made-up photonic quasicrystal.

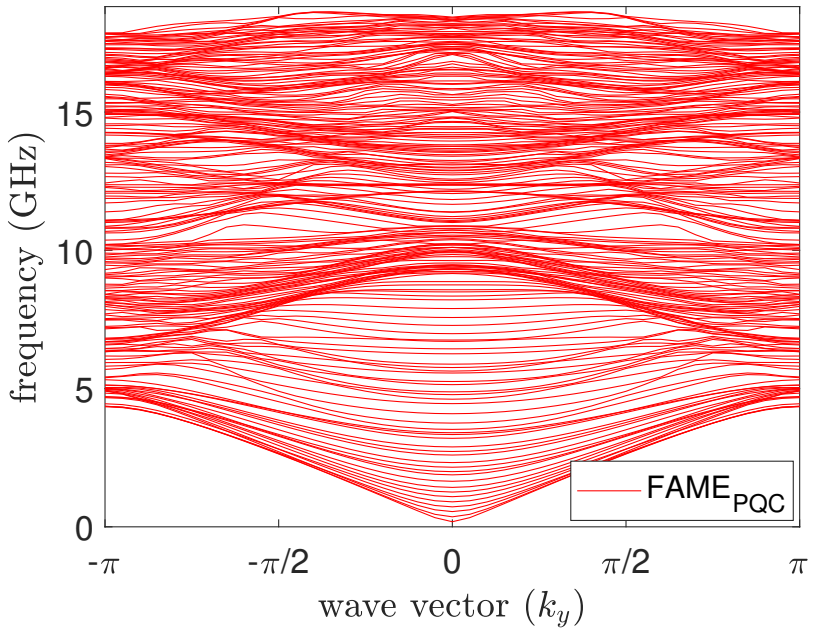

Figure 7: Band structure computed by FAME$_{PQC}$ for a made-up photonic quasicrystal approximated by the truncated Fibonacci (left, $\ell=13$) and Octonacci (right, $r=17$) sequence.

8 Conclusions

In this article, we adopt a bi-infinite approach to approximate 2D PQCs with 1D quasi-periodicity in order to compute photonic band structures. The basic idea is to first transform the discretized bi-infinite eigenvalue problem into a small scale finite-dimensional nonlinear eigenvalue problem (NEVP) via two-sided Schur's complement and then solve the NEVP by a nonlinear eigenvalue algorithm such as the nonlinear Jacobi-Davidson method which we use in our experiment. However, the NEVP is built upon the solutions to two systems of cyclic nonlinear matrix equations (NMEs). For that, we design the so-called *cyclic SDA* (C-SDA) consisting of an efficient coalescing technique followed by a structure-preserving doubling algorithm (SDA). The coalescing technique merges a system of N cyclic NMEs via just $\mathcal{O}(\log_\phi N)$ coalescing operations, instead of $O(N)$ ones, where ϕ is the generating ratio of the 1D quasiperiodic sequence of interest, e.g., ϕ is 1.618 for Fibonacci, 2.414 for Octonacci, and 2 for Thue-Morse. We name our complete method as FAME$_{PQC}$ to indicate that it is a sequel to our previous fast algorithms for photonic crystals. Results from our numerical experiments validate our approach in accuracy, in comparison with commercially available software COMSOL, and at the same time our method runs significantly faster and uses significantly less memory than COMSOL for very long sequences. Our analysis suggests, as well as demonstrated numeri-

cally, the computational complexity of our complete algorithm is $\mathcal{O}(n^2\log_\phi N)$ whereas that of COMSOL is $\mathcal{O}(n^2N)$, where n is the discretization scale of the scattering cell.

Acknowledgments

T. Li was partially supported by the National Natural Science Foundation of China (NSFC) No. 12371377 and the Jiangsu Provincial Scientific Research Center of Applied Mathematics under Grant No. BK20233002. Lyu was partially supported by Jiangsu Province Excellent Post-Doctoral Program 2023ZB142 in China. R.-C. Li was partially supported by US NSF DMS-2407692. T. Li and Lin were partially supported by Shanghai Institute for Mathematics and Interdisciplinary Sciences (SIMIS) under grant number SIMIS-ID-2024-LG. We thank Tianhe-2 and the Big Data Computing Center in Southeast University, China, for providing access to their computing resources.

A Review of SDA

SDA stands for structure-preserving doubling algorithm [12]. Recall NME (4.1): $X=Q-A^*(X-P)^{-1}A$, where $A,P,Q\in\mathbb{C}^{n\times n}$, $P=P^*$ and $Q=Q^*$. For $P=0$, it has been widely studied [19] (and references therein). The reader is referred to [12] for a general and comprehensive treatment, which is based on its equivalency to

$$\underbrace{\begin{bmatrix} A & 0 \\ -Q & I \end{bmatrix}}_{=:\mathscr{A}} \begin{bmatrix} I \\ X \end{bmatrix} = \underbrace{\begin{bmatrix} -P & I \\ -A^* & 0 \end{bmatrix}}_{=:\mathscr{B}} \begin{bmatrix} I \\ X \end{bmatrix} S, \tag{A.1}$$

where $S=(X-P)^{-1}A$. Equation (A.1) says that any solution X to (4.1) is closely related to an n-dimensional eigenspace of matrix pencil $\mathscr{A}-\nu\mathscr{B}$. This matrix pencil takes the so-called *second standard form* (SF2) [12, chapter 3] and is symplectic, i.e., $\mathscr{A}J\mathscr{A}^*=\mathscr{B}J\mathscr{B}^*$ [12, Theorem 3.4] where $J=\begin{bmatrix} 0 & I \\ -I & 0 \end{bmatrix}$. As a consequence, its eigenvalues appear in pairs that are "symmetrical" with respect to the unit circle (see, e.g., [12, Table 2.1]). For that reason, it has an even number of eigenvalues on the unit circle, if any. Artificially regarding half of those belonging to the closed unit disk and the other half to the complement of the open unit disk, we may say that symplectic pencil $\mathscr{A}-\nu\mathscr{B}$ always has n eigenvalues in the closed unit disk and the other n eigenvalues in the complement of the open unit disk. In particular, if it has no eigenvalues on the unit cycle, then it has n eigenvalues within the unit circle and n eigenvalues outside the unit circle.

A.1 SDA for the regular case

Often the desired solution X to (4.1) is the one for which S in (A.1) has all of its n eigenvalues lying in the closed unit disk. Numerically, SDA can find the desired solution

elegantly and effectively. Adopting the notation in [12], we write

$$\mathscr{A}_0 := \mathscr{A} \equiv \begin{bmatrix} E_0 & 0 \\ -X_0 & I \end{bmatrix}, \quad \mathscr{B}_0 := \mathscr{B} \equiv \begin{bmatrix} -Y_0 & I \\ -E_0^* & 0 \end{bmatrix}, \tag{A.2}$$

i.e., $E_0 = A$, $X_0 = Q = X_0^*$, and $Y_0 = P = Y_0^*$. We have, by (A.1), $\mathscr{A}_0 \begin{bmatrix} I \\ X \end{bmatrix} = \mathscr{B}_0 \begin{bmatrix} I \\ X \end{bmatrix} S$. SDA [12, Algorithm 3.2] iteratively computes $\mathscr{A}_k$ and $\mathscr{B}_k$ having the same structural form as the ones for $k=0$ such that

$$\mathscr{A}_k \begin{bmatrix} I \\ X \end{bmatrix} \equiv \begin{bmatrix} E_k & 0 \\ -X_k & I \end{bmatrix} \begin{bmatrix} I \\ X \end{bmatrix} = \begin{bmatrix} -Y_k & I \\ -E_k^* & 0 \end{bmatrix} \begin{bmatrix} I \\ X \end{bmatrix} S^{2^k} \equiv \mathscr{B}_k \begin{bmatrix} I \\ X \end{bmatrix} S^{2^k}, \tag{A.3}$$

where (E_k, X_k, Y_k) are recursively computed according to

$$E_{k+1} = E_k (X_k - Y_k)^{-1} E_k, \tag{A.4a}$$

$$X_{k+1} = X_k - E_k^* (X_k - Y_k)^{-1} E_k, \tag{A.4b}$$

$$Y_{k+1} = Y_k + E_k (X_k - Y_k)^{-1} E_k^*. \tag{A.4c}$$

These recursive formulas are well-defined, provided no $X_k - Y_k$ is singular.

It is important to note that X and S in (A.3) are the same ones as in (A.1). First we consider the case when $\mathscr{A} - \nu\mathscr{B}$ has no eigenvalues on the unit circle, which, in view of our earlier discussions, imply that $\mathscr{A} - \nu\mathscr{B}$ has exactly n eigenvalues in the open unit disk and the other n eigenvalues outside of the closed unit disk. The case is termed *the regular case* [12, section 3.7]. Let $\left[Z_1^{\mathrm{T}}, Z_2^{\mathrm{T}}\right]^{\mathrm{T}} \in \mathbb{C}^{2n\times n}$ be a basis matrix associated with the n eigenvalues in the open unit disk and suppose that $Z_1 \in \mathbb{C}^{n\times n}$ is invertible. Then there exists $\mathscr{M} \in \mathbb{C}^{n\times n}$ such that

$$\mathscr{A} \begin{bmatrix} Z_1 \\ Z_2 \end{bmatrix} = \mathscr{B} \begin{bmatrix} Z_1 \\ Z_2 \end{bmatrix} \mathscr{M} \Rightarrow \mathscr{A} \begin{bmatrix} I \\ Z_2 Z_1^{-1} \end{bmatrix} = \mathscr{B} \begin{bmatrix} I \\ Z_2 Z_1^{-1} \end{bmatrix} (Z_1 \mathscr{M} Z_1^{-1}), \tag{A.5}$$

i.e., (A.1) holds with $X = Z_2 Z_1^{-1}$ and $S = Z_1 \mathscr{M} Z_1^{-1}$ whose eigenvalues are the same as those of $\mathscr{M}$, which are the same as the n eigenvalues of $\mathscr{A} - \nu\mathscr{B}$ in the open unit disk. In particular, the spectral radius $\rho(S) < 1$. With such X and S in (A.3), we have

$$E_k = (X - Y_k) S^{2^k}, \;\; X - X_k = -E_k^* S^{2^k} \;\Rightarrow\; X - X_k = -[S^*]^{2^k} (X - Y_k) S^{2^k}.$$

Hence if $X - Y_k$ is uniformly bounded, then we will have

$$\lim_{k\to\infty} \|X - X_k\|^{1/2^k} \le [\rho(S)]^2. \tag{A.6}$$

Asymptotically, this says that $\|X - X_k\|$ goes to 0 as fast as $[\rho(S)]^{2^{k+1}} \to 0$, i.e., eventually quadratically. Inequality (A.6) essentially follows from the general convergence results in [12, section 3.7], where it is also shown that, under suitable conditions, Y_k converges to a solution of the dual equation of (4.1), implying that $X - Y_k$ is uniformly bounded. In summary, for the regular case, SDA is quadratically convergent.

A.2 SDA for the critical case

We consider the case when $\mathscr{A}-\nu\mathscr{B}$ has unimodular eigenvalues, the so-called *critical case* [12, section 3.8]. Earlier, we argued that the number of these unimodular eigenvalues must be even. To further simplify our analysis, we assume that these unimodular eigenvalues are semisimple, as this is the case for which SDA does not converge. Our analysis below for such a case will reveal a remedy to salvage the divergence by exploiting information from the SDA iterations (A.4).

Since we have assumed that all unimodular eigenvalues are semisimple, the Kronecker canonical form [6, Chapter IV] of $\mathscr{A}-\nu\mathscr{B}$ takes the form

$$W\mathscr{A}Z=\begin{bmatrix}J_1 & 0\\ 0 & I_n\end{bmatrix}\equiv J_{\mathscr{A}},\quad W\mathscr{B}Z=\begin{bmatrix}I_n & 0\\ 0 & J_2\end{bmatrix}\equiv J_{\mathscr{B}}, \tag{A.7}$$

where $W,Z\in\mathbb{C}^{2n\times 2n}$ are nonsingular, and

$$J_1=\Lambda\oplus J_s,\quad J_2=\Omega\oplus\bar{J}_s, \tag{A.8a}$$

$$\Lambda=\mathrm{diag}(e^{\imath\lambda_1},\cdots,e^{\imath\lambda_m}),\quad \Omega=\mathrm{diag}(e^{\imath\omega_1},\cdots,e^{\imath\omega_m}), \tag{A.8b}$$

$J_s\in\mathbb{C}^{(n-m)\times(n-m)}$ with the spectral radius $\rho(J_s)<1$. Since $J_{\mathscr{A}}$ and $J_{\mathscr{B}}$ commute, it holds from (A.7) that

$$\mathscr{A}ZJ_{\mathscr{B}}=W^{-1}J_{\mathscr{B}}J_{\mathscr{A}}=\mathscr{B}ZJ_{\mathscr{A}}. \tag{A.9}$$

By the doubling transformation theorem [12, Theorem 3.1(b)], we have

$$\mathscr{A}_kZJ_{\mathscr{B}}^{2^k}=\mathscr{B}_kZJ_{\mathscr{A}}^{2^k}. \tag{A.10}$$

In the same spirit as the proofs in [12, section 3.8], we now prove a convergence theorem for $\{\mathscr{A}_k-\nu\mathscr{B}_k\}_{k=1}^{\infty}$ generated by (A.4) for the current case.

Theorem A.1. *Let $\mathscr{A}-\nu\mathscr{B}$ be given as in* (A.1) *with all its unimodular eigenvalues being semisimple and admits the eigen-decompositions in* (A.7). *Suppose that $\{(E_k,X_k,Y_k)\}_{k=1}^{\infty}$ generated by the SDA recursion* (A.4) *is well-defined and that $\{E_k\}_{k=1}^{\infty}$ is uniformly bounded. Write Z in* (A.7) *as*

$$Z=\begin{bmatrix}Z_{11} & Z_{12}\\ Z_{21} & Z_{22}\end{bmatrix},\quad Z_{ij}\in\mathbb{C}^{n\times n},\quad i,j=1,2 \tag{A.11a}$$

and let

$$Z_{ij;1}:=Z_{ij(:,1:m)},\quad Z_{ij;2}=Z_{ij(:,m+1:n)},\quad i,j=1,2. \tag{A.11b}$$

If Z_{11} and Z_{12} are invertible, then we have

(i) $E_kZ_{11;2}=\mathcal{O}\big(\rho(J_s^{2^k})\big)\to 0$ *as* $k\to\infty$,

(ii) $X_k Z_{11;2} = Z_{21;2} + \mathcal{O}(\rho(J_s^{2^k})) \to Z_{21;2}$ *as* $k \to \infty$,

(iii) $Y_k Z_{12;2} = Z_{22;2} + \mathcal{O}(\rho(\bar{J}_s^{2^k})) \to Z_{22;2}$ *as* $k \to \infty$.

Proof. Plugging $\mathscr{A}_k - \nu\mathscr{B}_k$ in (A.3), $J_{\mathscr{A}}$ and $J_{\mathscr{B}}$ in (A.7) and Z in (A.11) into (A.10), we get

$$E_k Z_{11} = (-Y_k Z_{11} + Z_{21})(\Lambda^{2^k} \oplus J_s^{2^k}), \tag{A.12a}$$

$$E_k Z_{12}(\Omega^{2^k} \oplus \bar{J}_s^{2^k}) = -Y_k Z_{12} + Z_{22}, \tag{A.12b}$$

$$X_k Z_{11} - Z_{21} = E_k^* Z_{11}(\Lambda^{2^k} \oplus J_s^{2^k}), \tag{A.12c}$$

$$(X_k Z_{12} - Z_{22})(\Omega^{2^k} \oplus \bar{J}_s^{2^k}) = E_k Z_{12}. \tag{A.12d}$$

From (A.12b) it follows that

$$Y_k = Z_{22} Z_{12}^{-1} - E_k Z_{12}(\Omega^{2^k} \oplus \bar{J}_s^{2^k}) Z_{12}^{-1}, \tag{A.13}$$

which implies that Y_k is uniformly bounded because E_k is assumed uniformly bounded and the spectral norm $\|\Omega^{2^k}\|_2 = 1$ always and $\bar{J}_s^{2^k} \to 0$ as $k \to \infty$. By (A.12a), we get

$$E_k Z_{11;2} = (-Y_k Z_{11} + Z_{21}) \begin{bmatrix} 0 \\ J_s^{2^k} \end{bmatrix} = \mathcal{O}\big(\rho(J_s^{2^k})\big) \to 0 \quad \text{as } k \to \infty.$$

This proves item (i). By (A.12c), we have

$$\begin{aligned} X_k &= Z_{21} Z_{11}^{-1} + E_k^* Z_{11}\big(\Lambda^{2^k} \oplus J_s^{2^k}\big) Z_{11}^{-1} \\ &= Z_{21} Z_{11}^{-1} + \widehat{U}_k V_{11;1}^{\mathrm{T}} + \mathcal{O}\big(\rho(J_s^{2^k})\big) \end{aligned}$$

for some uniformly bounded matrix $\widehat{U}_k \in \mathbb{C}^{n \times m}$, and then it holds that

$$X_k Z_{11;2} = Z_{21} \begin{bmatrix} 0 \\ I_{n-m} \end{bmatrix} + \mathcal{O}\big(\rho(J_s^{2^k})\big) = Z_{21;2} + \mathcal{O}\big(\rho(J_s^{2^k})\big) \to Z_{21;2}$$

as $k \to \infty$, proving item (ii). Similarly, from (A.12b), we also have

$$Y_k Z_{12;2} = Z_{22;2} + \mathcal{O}(\rho(\bar{J}_s^{2^k})) \to Z_{22;2} \quad \text{as } k \to \infty,$$

as expected for item (iii). □

In the critical case, X_k does not converge in its entirety, but some component of it does. The problem is how to exploit the converging component so as to construct the desired weakly stable solution. This is what we will do in the following. From Theorem A.1(i, ii), we find that

$$\begin{bmatrix} Z_{11;2} \\ Z_{21;2} \end{bmatrix} \approx \begin{bmatrix} Z_{11;2} \\ X_k Z_{11;2} \end{bmatrix} \tag{A.14}$$

forms an approximate stable invariant subspace of $\mathscr{A}-\nu\mathscr{B}$ corresponding to J_s. Usually after just 8 to 10 SDA iterations (A.4), $Z_{11;2}$ computed by the SVD of E_k such that $E_kZ_{11;2}\approx 0$ is accurate enough.

But we have to construct $Z_{11;1}$ and $Z_{21;1}$. To that end, we perturb $\mathscr{A}-\nu\mathscr{B}$ to $\widetilde{\mathscr{A}}-\nu\widetilde{\mathscr{B}}$:

$$\widetilde{\mathscr{A}}=\begin{bmatrix}\widetilde{A} & 0\\ -\widetilde{Q} & I\end{bmatrix},\quad \widetilde{\mathscr{B}}=\begin{bmatrix}-\widetilde{P} & I\\ \widetilde{B} & 0\end{bmatrix}, \tag{A.15a}$$

where, for some sufficiently small η, say $\eta\approx 10^{-8}$,

$$\widetilde{A}=A+\imath\eta D,\quad \widetilde{B}=-A^*-\imath\eta D^*,\quad \widetilde{Q}=Q+\imath\eta I,\quad \widetilde{P}=P-\imath\eta I, \tag{A.15b}$$

and D is specially chosen to fit the structure of A in (A.1) coming from the FEM discretization in Section 2 as follows:

$$A=\begin{bmatrix}0 & A_0\\ 0 & 0\end{bmatrix},\quad D=\begin{bmatrix}0 & I\\ 0 & 0\end{bmatrix}. \tag{A.15c}$$

In (A.15c), by virtue of FEM, A_0 at the top-right corner of A has relatively a very small size, and the identity matrix at the top-right corner of D is made to have the same size as A_0. Hence $\widetilde{A}$ preserve the same structure in A. Based on the result of [10], the matrix pair $\widetilde{\mathscr{A}}-\nu\widetilde{\mathscr{B}}$ of (A.15a) can be made to have no eigenvalue on the unit circle, as guaranteed by the next theorem.

Theorem A.2. *Suppose that $2I-\nu D^*-\bar{\nu}D$ is positive definite for all $\nu\in\mathbb{T}$ (the unit circle). Then for any $\eta\neq 0$, $\widetilde{\mathscr{A}}-\nu\widetilde{\mathscr{B}}$ in* (A.15) *has n eigenvalues inside the open unit disk and n eigenvalues outside of the closed unit disk.*

Proof. Suppose that there is some $\nu_0\in\mathbb{T}$ and $x=[x_1^{\mathrm{T}},x_2^{\mathrm{T}}]^{\mathrm{T}}$ with $x_1,x_2\in\mathbb{C}^n$ such that $\widetilde{\mathscr{A}}x=\nu_0\widetilde{\mathscr{B}}x$. Then

$$\widetilde{A}x_1=\nu_0(-\widetilde{P}x_1+x_2),\quad -\widetilde{Q}x_1+x_2=\nu_0\widetilde{B}x_1. \tag{A.16}$$

From the second equation in (A.16), we get $x_2=\widetilde{Q}x_1+\nu_0\widetilde{B}x_1$. By the first equation in (A.16), we have $\bar{\nu}_0\widetilde{A}x_1-x_2=-\widetilde{P}x_1$, and thus

$$(\bar{\nu}_0\widetilde{A}-\widetilde{Q}-\nu_0\widetilde{B})x_1=-\widetilde{P}x_1,$$

pre-multiplying which by x_1^*, upon using (A.15b), yields

$$x_1^*\left[\nu_0(A^*+\imath\eta D^*)+\bar{\nu_0}(A+\imath\eta D)-(Q+\imath\eta I))\right]x_1=-x_1^*(P-\imath\eta I)x_1. \tag{A.17}$$

Examining the imaginary part at the both sides of (A.17) leads to $\eta x_1^*(\nu_0D^*+\bar{\nu_0}D-2I)x_1=0$. Since $2I-\nu_0D^*-\bar{\nu_0}D$ is positive definite by assumption, it implies that $x_1=0$ and thus also $x_2=0$ by (A.16). Therefore $\widetilde{\mathscr{A}}-\nu\widetilde{\mathscr{B}}$ has no eigenvalues on $\mathbb{T}$.

Algorithm A.2 C-SDA for solving (4.8).

Input: defining matrices A_i, P_i, Q_i for $1\le i\le r$ of cyclic NMEs (4.8);
Output: the X_1-component of solution $(X_1,X_2,\cdots,X_r)$ to NMEs (4.8).

1: coalesce NMEs (4.8) to (4.1), according to Section 4;
2: initialize $\mathscr{A}_0$ and $\mathscr{B}_0$ as in (A.2);
3: perform SDA iteration according to (A.4) for $k_{\max}$ steps;
4: **if** non-convergence is detected **then**
5: perturb A, Q, P to get $\widetilde{A}$, $\widetilde{B}$, $\widetilde{Q}$, $\widetilde{P}$ as in (A.15), and initialize $\widetilde{\mathscr{A}_0}$, $\widetilde{\mathscr{B}}_0$ as in (A.19);
6: perform SDA iteration according to (A.21) for $k_{\max}$ steps;
7: compute the largest eigenvalues $\{\widetilde{\nu}_i\}_{i=1}^m$ in absolute value of $(\widetilde{X}-\widetilde{P})^{-1}\widetilde{A}$;
8: compute the unimodular eigenpairs $\{(\nu_i,\mathbf{z}_i)\}_{i=1}^m$ for $\mathscr{A}-\nu\mathscr{B}$ with $\{\widetilde{\nu}_i\}_{i=1}^m$ as initial guesses by the inverse iteration;
9: construct Z_1 and Z_2 as in (A.22);
10: **return** $Z_2Z_1^{-1}$;
11: **else**
12: **return** last approximate solution to (4.1) from Step 3.
13: **end if**

We now consider the matrix pencil parameterized by $t\in[0,1]$

$$\widetilde{\mathscr{A}}(t)-\nu\widetilde{\mathscr{B}}(t):=\begin{bmatrix}t(A+\imath\eta D) & 0\\ -(Q+\imath\eta I) & I\end{bmatrix}-\nu\begin{bmatrix}-P+\imath\eta I & I\\ -t(A^*+\imath\eta D^*) & 0\end{bmatrix}. \tag{A.18}$$

For each $t\in[0,1]$ and $\nu\in\mathbb{T}$,

$$2I-\nu(tD^*)-\bar{\nu}(tD)=2(1-t)I+t(2I-\nu D^*-\bar{\nu}D)\succ 0.$$

By the same argument for $\widetilde{\mathscr{A}}-\nu\widetilde{\mathscr{B}}$ above, we conclude that $\widetilde{\mathscr{A}}(t)-\nu\widetilde{\mathscr{B}}(t)$ has no eigenvalues on $\mathbb{T}$ for all $t\in[0,1]$. It is clear that $\widetilde{\mathscr{A}}(0)-\nu\widetilde{\mathscr{B}}(0)$ has n eigenvalues at 0 and n eigenvalues at ∞. Since the eigenvalues of matrix pencil are continuous with respect to matrix entries [18,31], $\widetilde{\mathscr{A}}(t)-\nu\widetilde{\mathscr{B}}(t)$ has the same number of eigenvalues inside the open unit disk for all $t\in[0,1]$, i.e., n, and its other n eigenvalues are outside of the closed unit disk for all $t\in[0,1]$. We conclude that $\widetilde{\mathscr{A}}-\nu\widetilde{\mathscr{B}}=\widetilde{\mathscr{A}}(1)-\nu\widetilde{\mathscr{B}}(1)$ in (A.15) has n eigenvalues inside the open unit disk and n eigenvalues outside of the closed unit disk. □

Like $\mathscr{A}-\nu\mathscr{B}$ in (A.1), $\widetilde{\mathscr{A}}-\nu\widetilde{\mathscr{B}}$ in (A.15) also takes the forms of (SF2) [12, chapter 3] but it is no longer symplectic. Still, by Theorem A.2, it has n eigenvalues inside the open unit disk and n eigenvalues outside of the closed unit disk, falling into *the regular case* [12, section 3.7]. Let $\left[\widetilde{Z}_1^{\mathrm{T}},\widetilde{Z}_2^{\mathrm{T}}\right]^{\mathrm{T}}\in\mathbb{C}^{2n\times n}$ be a basis matrix associated with the n eigenvalues in the open unit disk and suppose that $\widetilde{Z}_1\in\mathbb{C}^{n\times n}$ is invertible. Similarly to (A.5) there exists $\widetilde{\mathscr{M}}\in\mathbb{C}^{n\times n}$ such that

$$\widetilde{\mathscr{A}}\begin{bmatrix}\widetilde{Z}_1\\ \widetilde{Z}_2\end{bmatrix}=\widetilde{\mathscr{B}}\begin{bmatrix}\widetilde{Z}_1\\ \widetilde{Z}_2\end{bmatrix}\widetilde{\mathscr{M}}\Rightarrow\widetilde{\mathscr{A}}\begin{bmatrix}I\\ \widetilde{Z}_2\widetilde{Z}_1^{-1}\end{bmatrix}=\widetilde{\mathscr{B}}\begin{bmatrix}I\\ \widetilde{Z}_2\widetilde{Z}_1^{-1}\end{bmatrix}(\widetilde{Z}_1\widetilde{\mathscr{M}}\widetilde{Z}_1^{-1}),$$

where the eigenvalues of $\widetilde{S}:=\widetilde{Z}_1\widetilde{\mathscr{M}}\widetilde{Z}_1^{-1}$ are in the open unit disk. The doubling algorithm for (SF2) [12, Algorithm 3.2] can be readily applied to compute $\widetilde{X}:=\widetilde{Z}_2\widetilde{Z}_1^{-1}$. Specifically, adopting the notation in [12], we write

$$\widetilde{\mathscr{A}_0}:=\widetilde{\mathscr{A}}\equiv\begin{bmatrix}\widetilde{E}_0 & 0\\ -\widetilde{X}_0 & I\end{bmatrix},\quad \widetilde{\mathscr{B}}_0:=\widetilde{\mathscr{B}}\equiv\begin{bmatrix}-\widetilde{Y}_0 & I\\ \widetilde{F}_0 & 0\end{bmatrix},\tag{A.19}$$

i.e., $\widetilde{E}_0=\widetilde{A}$, $\widetilde{X}_0=\widetilde{Q}$, $\widetilde{F}_0=\widetilde{B}$, and $\widetilde{Y}_0=\widetilde{P}$. We have, by (A.1), $\widetilde{\mathscr{A}_0}\begin{bmatrix}I\\ \widetilde{X}\end{bmatrix}=\widetilde{\mathscr{B}}_0\begin{bmatrix}I\\ \widetilde{X}\end{bmatrix}\widetilde{S}$. Again SDA [12, Algorithm 3.2] iteratively computes $\widetilde{\mathscr{A}_k}$ and $\widetilde{\mathscr{B}}_k$ having the same structural form as the ones for $k=0$ such that

$$\widetilde{\mathscr{A}_k}\begin{bmatrix}I\\ \widetilde{X}\end{bmatrix}\equiv\begin{bmatrix}\widetilde{E}_k & 0\\ -\widetilde{X}_k & I\end{bmatrix}\begin{bmatrix}I\\ \widetilde{X}\end{bmatrix}=\begin{bmatrix}-\widetilde{Y}_k & I\\ \widetilde{F}_k & 0\end{bmatrix}\begin{bmatrix}I\\ \widetilde{X}\end{bmatrix}\widetilde{S}^{2^k}\equiv\widetilde{\mathscr{B}}_k\begin{bmatrix}I\\ \widetilde{X}\end{bmatrix}\widetilde{S}^{2^k},\tag{A.20}$$

where $(\widetilde{E}_k,\widetilde{F}_k,\widetilde{X}_k,\widetilde{Y}_k)$ are recursively computed according to

$$\widetilde{E}_{k+1}=\widetilde{E}_k(\widetilde{X}_k-\widetilde{Y}_k)^{-1}\widetilde{E}_k,\tag{A.21a}$$
$$\widetilde{F}_{k+1}=\widetilde{F}_k(\widetilde{Y}_k-\widetilde{X}_k)^{-1}F_k,\tag{A.21b}$$
$$\widetilde{X}_{k+1}=\widetilde{X}_k+\widetilde{F}_k(\widetilde{X}_k-\widetilde{Y}_k)^{-1}\widetilde{E}_k,\tag{A.21c}$$
$$\widetilde{Y}_{k+1}=\widetilde{Y}_k+\widetilde{E}_k(\widetilde{Y}_k-\widetilde{X}_k)^{-1}\widetilde{F}_k.\tag{A.21d}$$

These recursive formulas are well-defined, provided no $\widetilde{X}_k-\widetilde{Y}_k$ is singular.

At convergence, $\widetilde{X}_k$ goes to the stabilizing solution $\widetilde{X}$ such that $\widetilde{S}=(\widetilde{X}-\widetilde{P})^{-1}\widetilde{A}$ with $\rho(\widetilde{S})<1$ and $\widetilde{X}+\widetilde{B}(\widetilde{X}-\widetilde{P})^{-1}\widetilde{A}=\widetilde{Q}$. Then we compute the largest eigenvalues $\widetilde{\nu}_1,\cdots,\widetilde{\nu}_m$ in absolute value of $\widetilde{S}$. The rationale is that these are the ones associated with the unimodular eigenvalues $\{\nu_i\}_{i=1}^m$, albeit unknown, of $\mathscr{A}-\nu\mathscr{B}$ that are moved to the inside of the open unit disk by the perturbations in (A.15). We then perform the inverse iteration [8] to compute the unimodular eigenpairs $\{(\nu_i,\mathbf{z}_i)\}_{i=1}^m$ for $\mathscr{A}-\nu\mathscr{B}$ with $\{\widetilde{\nu}_i\}_{i=1}^m$ as initial guesses, respectively. Set

$$\begin{bmatrix}Z_{11;1}\\ Z_{21;1}\end{bmatrix}=[\mathbf{z}_1,\cdots,\mathbf{z}_m],\quad \begin{bmatrix}Z_1\\ Z_2\end{bmatrix}=\begin{bmatrix}Z_{11;1} & Z_{11;2}\\ Z_{21;1} & Z_{21;2}\end{bmatrix},\tag{A.22}$$

where $Z_{11;2}$ and $Z_{21;2}$ are from (A.14). Finally, the desired stabilizing solution X for (4.1) is obtained by $X=Z_2Z_1^{-1}$. The new SDA variant for solving (4.1) is summarized into a part of Algorithm A.2.

B F_{C}' by solving cyclic Stein equations

Differentiating $F_{\mathrm{C}}(\nu)$ of (3.20) with respect to ν at θ, we get

$$\begin{aligned}F_{\mathrm{C}}'(\theta)=&-M_{\mathrm{C}}+\widehat{F}_{\mathrm{C}}\widehat{G}_1(\theta)(\widehat{E}_{\mathrm{C}}-\theta\widehat{F}_{\mathrm{C}})^*+(\widehat{E}_{\mathrm{C}}-\theta\widehat{F}_{\mathrm{C}})\widehat{G}_1(\theta)\widehat{F}_{\mathrm{C}}^*\\&+F_{\mathrm{C}}^*G_1(\theta)(E_{\mathrm{C}}-\theta F_{\mathrm{C}})+(E_{\mathrm{C}}-\theta F_{\mathrm{C}})^*G_1(\theta)F_{\mathrm{C}}\\&-(\widehat{E}_{\mathrm{C}}-\theta\widehat{F}_{\mathrm{C}})\widehat{G}_1'(\theta)(\widehat{E}_{\mathrm{C}}-\theta\widehat{F}_{\mathrm{C}})^*-(E_{\mathrm{C}}-\theta F_{\mathrm{C}})^*G_1'(\theta)(E_{\mathrm{C}}-\theta F_{\mathrm{C}}),\end{aligned}\tag{B.1}$$

which depends on $G_1'(\theta)$ and $\widehat{G}_1'(\theta)$. It is known that

$$\big[G_j(\theta)^{-1}\big]'=-G_j(\theta)^{-1}G_j'(\theta)G_j(\theta)^{-1},\ \big[\widehat{G}_j(\theta)^{-1}\big]'=-\widehat{G}_j(\theta)^{-1}\widehat{G}_j'(\theta)\widehat{G}_j(\theta)^{-1}$$

yielding

$$G_j'(\theta)=-G_j(\theta)\big[G_j(\theta)^{-1}\big]'G_j(\theta),\quad \widehat{G}_j'(\theta)=-\widehat{G}_j(\theta)\big[\widehat{G}_j(\theta)^{-1}\big]'\widehat{G}_j(\theta).\tag{B.2}$$

Differentiate (4.2) and (4.3) with respect to ν at θ, respectively, we get

$$\begin{aligned}\big[G_j(\theta)^{-1}\big]'=&-\theta M_j+F_j^*G_{j+1}(\theta)(E_j-\theta F_j)\\&+(E_j-\theta F_j)^*G_{j+1}(\theta)F_j-(E_j-\theta F_j)^*G_{j+1}'(\theta)(E_j-\theta F_j),\end{aligned}\tag{B.3}$$

for $j=1,\cdots,r$, where $G_{r+1}(\cdot)\equiv G_1(\cdot)$, and

$$\begin{aligned}\big[\widehat{G}_j(\theta)^{-1}\big]'=&\big(-\theta\widehat{M}_j+\widehat{F}_j\widehat{G}_{j+1}(\theta)(\widehat{E}_j-\theta\widehat{F}_j)^*\big)\\&+(\widehat{E}_j-\theta\widehat{F}_j)\widehat{G}_{j+1}(\theta)\widehat{F}_j^*-(\widehat{E}_j-\theta\widehat{F}_j)\widehat{G}_{j+1}'(\theta)(\widehat{E}_j-\theta\widehat{F}_j)^*,\end{aligned}\tag{B.4}$$

for $j=1,\cdots,\ell$, where $\widehat{G}_{\ell+1}(\cdot)\equiv\widehat{G}_1(\cdot)$. Let

$$Y_j=G_j'(\theta),\widehat{Y}_j=\widehat{G}_j'(\theta).$$

Let $B_j=G_j(\theta)(E_j-\theta F_j)^*$. Combine (B.2) and (B.3) to get

$$\begin{aligned}Y_j-B_j^*Y_{j+1}B_j&=G_j'(\theta)-\big[G_j(\theta)(E_j-\theta F_j)^*\big]G_{j+1}'(\theta)\big[(E_j-\theta F_j)G_j(\theta)\big]\\&=G_j(\theta)\big[\theta M_j-F_j^*G_{j+1}(\theta)(E_j-\theta F_j)-(E_j-\theta F_j)^*G_{j+1}(\theta)F_j\big]G_j(\theta)\\&=:H_j,\end{aligned}\tag{B.5}$$

for $j=1,\cdots,r$, where $Y_{r+1}=Y_1$. Similarly, let $\widehat{B}_j=\widehat{G}_j(\theta)(\widehat{E}_j-\theta\widehat{F}_j)$. Now combine (B.2) and (B.4) to get

$$\begin{aligned}\widehat{Y}_j-\widehat{B}_j\widehat{Y}_{j+1}\widehat{B}_j^*&=\widehat{G}_j'(\theta)-\big[\widehat{G}_j(\theta)(\widehat{E}_j-\theta\widehat{F}_j)\big]\widehat{G}_{j+1}'(\theta)\big[(\widehat{E}_j-\theta\widehat{F}_j)^*\widehat{G}_j(\theta)\big]\\&=\widehat{G}_j(\theta)\big[\theta\widehat{M}_j-\widehat{F}_j\widehat{G}_{j+1}(\theta)(\widehat{E}_j-\theta\widehat{F}_j)^*-(\widehat{E}_j-\theta\widehat{F}_j)\widehat{G}_{j+1}(\theta)\widehat{F}_j^*\big]\widehat{G}_j(\theta)\\&=:\widehat{H}_j,\end{aligned}\tag{B.6}$$

for $j=1,\cdots,\ell$, where $\widehat{Y}_{\ell+1}=\widehat{Y}_1$. We now have two systems of cyclic Stein equations in (B.5) and (B.6). A similar coalescing technique to that in Section 4 can be developed to yield

$$Y_1 - A_\alpha^* Y_1 A_\alpha = H_\alpha, \tag{B.7a}$$

$$\widehat{Y}_1 - \widehat{A}_{\widehat{\alpha}} \widehat{Y}_1 \widehat{A}_{\widehat{\alpha}}^* = \widehat{H}_{\widehat{\alpha}}. \tag{B.7b}$$

The equations in (B.7) can be solved by essentially Smith's method [29], a special case of another type of SDA specialized to the Sylvester equation (see, e.g., [37, section 4] for explanation).

References

[1] W. N. Anderson, Jr., T. D. Morley, and G. E. Trapp. Positive solutions to $X = A - BX^{-1}B^*$. *Linear Algebra and its Applications*, 234:53–62, 1990.

[2] S. Datta. *Electronic Transport in Mesoscopic Systems*. Cambridge University Press, 1997.

[3] E. N. Economou. *Green's Functions in Quantum Physics*, volume 7. Springer Science & Business Media, 2006.

[4] K. Edagawa. Photonic crystals, amorphous materials, and quasicrystals. *Science and Technology of Advanced Materials*, 15(3):034805, 2014.

[5] J. C. Engwerda, A. C. M. Ran, and A. L. Rijkeboer. Necessary and sufficient conditions for the existence of a positive definite solution of the matrix equation $X + A^* X^{-1} A = Q$. *Linear Algebra and its Applications*, 186:255–275, 1993.

[6] F. R. Gantmacher. The Theory of Matrices, vol. 2, 1959. *Chelsea, New York*, 2000.

[7] I. Gohberg, S. Goldberg, and M. A. Kaashoek. *Classes of Linear Operators*, volume 63. Birkhäuser, 2013.

[8] Gene H. Golub and Qiang Ye. Inexact inverse iteration for generalized eigenvalue problems. *BIT*, 40(4):671–684, 2000.

[9] C.-H. Guo, Y.-C. Kuo, and W.-W. Lin. Complex symmetric stabilizing solution of the matrix equation $X + A^\top X^{-1} A = Q$. *Linear Algebra and its Applications*, 435(6):1187–1192, 2011.

[10] C.-H. Guo, Y.-C. Kuo, and W.-W. Lin. Numerical solution of nonlinear matrix equations arising from Green's function calculations in nano research. *J. Comput. Appl. Math.*, 236(17):4166–4180, 2012.

[11] C.-H. Guo, Y.-C. Kuo, and W.-W. Lin. On a nonlinear matrix equation arising in nano research. *SIAM Journal on Matrix Analysis and Applications*, 33(1):235–262, 2012.

[12] T.-M. Huang, R.-C. Li, and W.-W. Lin. *Structure-Preserving Doubling Algorithms for Nonlinear Matrix Equations*. SIAM, 2018.

[13] C. Janot. Quasicrystals. In *Neutron and Synchrotron Radiation for Condensed Matter Studies: Applications to Solid State Physics and Chemistry*, pages 197–211. Springer, 1994.

[14] K. Jiang and P. Zhang. Numerical methods for quasicrystals. *J. Comput. Phys.*, 256:428–440, 2014.

[15] J. D. Joannopoulos, S. G. Johnson, J. N. Winn, and R. D. Meade. *Photonic Crystals: Molding the Flow of Light*. Princeton University Press, Princeton, NJ, 2008.

[16] D. L. John and D. L. Pulfrey. Green's function calculations for semi-infinite carbon nanotubes. *Physica Status Solidi (B)*, 243(2):442–448, 2006.

[17] C. Kittel. *Introduction to Solid State Physics*. Wiley, New York, NY, 2005.

[18] R.-C. Li. On perturbation theorems for the generalized eigenvalues of regular matrix pencils. *Mathematica Numerica Sinica*, 11:10–19, 1989. In Chinese. Engl. trans. in *Chinese Journal of Numerical Mathematics and Applications* **11** (1989) 24-35.
[19] W.-W. Lin and S.-F. Xu. Convergence analysis of structure-preserving doubling algorithms for Riccati-type matrix equations. *SIAM J. Matrix Anal. Appl.*, 28(1):26–39, 2006.
[20] Q. Liu, H.-N. Yang, T. Li, H. Tian, and Z. Yang. An efficient and unified method for band structure calculations of 2D anisotropic photonic-crystal fibers. *Calcolo*, 61(2):20, 2024.
[21] X.-L. Lyu, T. Li, J.-W. Lin, T.-M. Huang, W.-W. Lin, and H. Tian. Solving Maxwell eigenvalue problems for three dimensional isotropic photonic crystals with fourteen Bravais lattices. *Journal of Computational and Applied Mathematics*, 410:114220, 2022.
[22] E. Maciá-Barber. *Quasicrystals: Fundamentals and Applications*. CRC Press, 2020.
[23] A. N. Poddubny and E. L. Ivchenko. Photonic quasicrystalline and aperiodic structures. *Physica E: Low-dimensional Systems and Nanostructures*, 42(7):1871–1895, 2010.
[24] M. C. Rechtsman, H.-C. Jeong, P. M. Chaikin, S. Torquato, and P. J. Steinhardt. Optimized structures for photonic quasicrystals. *Phys. Rev. Lett.*, 101(7):073902, 2008.
[25] A. W. Rodriguez, A. P. McCauley, Y. Avniel, and S. G. Johnson. Computation and visualization of photonic quasicrystal spectra via Bloch's theorem. *Physical Review B—Condensed Matter and Materials Physics*, 77(10):104201, 2008.
[26] A. Shi, Y. Peng, J. Jiang, Y. Peng, P. Peng, J. Chen, H. Chen, S. Wen, X. Lin, F. Gao, et al. Observation of topological corner state arrays in photonic quasicrystals. *Laser & Photonics Reviews*, page 2300956, 2024.
[27] G. Sleijpen and H. van der Vorst. Jacobi-Davidson method. In Zhaojun Bai, J. Demmel, J. Dongarra, A. Ruhe, and H. van der Vorst, editors, *Templates for the Solution of Algebraic Eigenvalue Problems: A Practical Guide*, pages 238–246. SIAM, 2000.
[28] G. L. G. Sleijpen and H. A. van der Vorst. A Jacobi-Davidson iteration method for linear eigenvalue problems. *SIAM Journal on Matrix Analysis and Applications*, 17:401–425, 1996.
[29] R. A. Smith. Matrix equation $XA+BX=C$. *SIAM Journal on Applied Mathematics*, 16(1):198–201, 1968.
[30] W. Steurer and D. Sutter-Widmer. Photonic and phononic quasicrystals. *Journal of Physics D: Applied Physics*, 40(13):R229, 2007.
[31] G. W. Stewart and J.-G. Sun. *Matrix Perturbation Theory*. Academic Press, New York, New York, 1990.
[32] Wu-Pei Su, John Robert Schrieffer, and Alan J Heeger. Solitons in polyacetylene. *Physical Review Letters*, 42(25):1698, 1979.
[33] H. Tian, T. Li, X.-L. Lyu, and W.-W. Lin. Band structure calculations of three-dimensional anisotropic photonic crystals in the oblique coordinate system. *SIAM Journal on Scientific Computing*, 45(4):B440–B466, 2023.
[34] Z. V. Vardeny, A. Nahata, and A. Agrawal. Optics of photonic quasicrystals. *Nature Photonics*, 7(3):177–187, 2013.
[35] H. Voss. A Jacobi–Davidson method for nonlinear and nonsymmetric eigenproblems. *Computers & Structures*, 85(17-18):1284–1292, 2007.
[36] K. Wang, S. David, A. Chelnokov, and J. M. Lourtioz. Photonic band gaps in quasicrystal-related approximant structures. *Journal of Modern Optics*, 50(13):2095–2105, 2003.
[37] W.-G. Wang, W.-C. Wang, and R.-C. Li. Alternating-directional doubling algorithm for M-matrix algebraic Riccati equations. *SIAM Journal on Matrix Analysis and Applications*, 33:170–194, 2012.
[38] Bi-Ye Xie, Hong-Fei Wang, Hai-Xiao Wang, Xue-Yi Zhu, Jian-Hua Jiang, Ming-Hui Lu, and

Yan-Feng Chen. Second-order photonic topological insulator with corner states. *Physical Review B*, 98(20):205147, 2018.

[39] Y. Zhang, Z. Che, W. Liu, J. Wang, M. Zhao, F. Guan, X. Liu, L. Shi, and J. Zi. Unfolded band structures of photonic quasicrystals and moiré superlattices. *Physical Review B*, 105(16):165304, 2022.